Transition probabilities between high spin states in ^{88}Mo and ^{90}Mo

M.K. Kabadiyski, C.J. Gross,*A. Harder, K.P. Lieb, D. Rudolph, and M. Weiszflog
II. Physikalisches Institut, Universität Göttingen, D-37073 Göttingen, Germany

J. Altmann, A. Dewald, J. Eberth, and T. Mylaeus
Institut für Kernphysik der Universität zu Köln, D-50937 Köln, Germany

H. Grawe, J. Heese, and K.-H. Maier
Hahn-Meitner-Institut GmbH, D-14109 Berlin, Germany
(Received 2 February 1994)

The reactions ^{58}Ni(^{36}Ar, $\alpha 2p$)^{88}Mo and ^{58}Ni(^{36}Ar, $4p$)^{90}Mo at 149 and 140 MeV beam energies have been used to carry out Doppler shift attenuation and recoil distance lifetime measurements and to determine DCO ratios in ^{88}Mo and ^{90}Mo. A singles angular distribution experiment using the reaction ^{58}Ni(^{35}Cl,$3p$)^{90}Mo has been performed at 120 MeV beam energy to measure spin assignments in ^{90}Mo and to calibrate the DCO analyses for both nuclei. Reduced transition probabilities for more than 60 transitions in ^{88,90}Mo have been deduced. The extensive data set is incorporated in a detailed comparison between the two nuclei and, for ^{90}Mo, with predictions from shell model calculations within a restricted $\pi(p_{1/2})$, $\pi(g_{9/2})$, $\nu(p_{1/2})$, and $\nu(g_{9/2})$ configuration space and with different residual interaction parameters. The electromagnetic properties of the negative parity states of ^{90}Mo are well reproduced by the calculations while the positive parity states show hints of seniority mixing at intermediate spins.

PACS number(s): 21.10.Tg, 21.60.Cs, 27.50.+e, 27.60.+j

I. INTRODUCTION

The high spin spectra of many nuclides with proton number $Z = 40$–44 and neutron number $N = 46$–49 have been recently studied with heavy ion fusion evaporation reactions [1–14]. When interpreting the level energies and γ-ray branching ratios using the spherical shell model, it was found that, even within the $(1g_{9/2}, 2p_{1/2})$ model space, most features could be understood surprisingly well. Effective single-particle energies and two-body matrix elements derived by Gross and Frenkel [15] were used. In simple terms, the large number of $g_{9/2}$ proton particles and neutron holes, relative to the semimagic ^{88}Sr core, provides high spins via single-particle angular momentum alignment, without the need of collective excitation. The high spin states can be grouped into shell model configurations of fixed seniority $v = v_\pi + v_\nu$ where v_π and v_ν are the proton and neutron seniorities, respectively. Most of these states are connected by $E2$ and (fast) $M1$ radiations of single-particle strengths, but occasionally the predominant proton and neutron parts of the wave functions are coupled to seniorities and spins which do not allow γ decays to take place. This may result in strongly hindered transitions and long lifetimes; we refer here to these as seniority isomers.

The high spin spectrum of ^{90}Mo ($Z = 42$, $N = 48$) has been established by several groups [7,16–18]. The most comprehensive level scheme given by Kabadiyski *et al.* [7], as well as that of Arnell *et al.* [16], reaches beyond $I^\pi = 20^+$ which is the highest value accessible within the $[\pi(g_{9/2})^4\nu(g_{9/2})^{-2}]$ configuration. To account for the observed yrast states of higher spins ($I \leq 25\hbar$), promotion of up to two protons from the $(2p_{3/2}, f_{5/2})$ orbits is required [7,10]. Weiszflog *et al.* [19] have recently reported the measurement of g-factors and the interpretation of some excited states in ^{90}Mo. The ground state band in ^{88}Mo has been identified first by Gross *et al.* [2]; high spin states have been extended by Weiszflog *et al.* [5] up to probable spins $I^\pi = 22^+$ and $I^\pi = 23^-$.

The aim of the present study is to complement the existing level schemes and γ-ray branching ratios in both nuclei by the measurement of $E2/M1$ mixing ratios and lifetimes, from which, a large number of precise transition probabilities are deduced. These quantities serve as a very stringent test of the predicted shell model wave functions. In Sec. II, we present the experimental techniques and reduction of multipole mixing ratios and partial lifetimes via Doppler shift attenuation and recoil distance methods. A detailed comparison between the two nuclei is presented in Sec. III. Shell model calculations on ^{90}Mo using different model parameters are discussed in Sec. IV, while the interpretation of the ^{88}Mo results will be given in a forthcoming paper.

II. EXPERIMENTS AND DATA REDUCTION

The transition probabilities in ^{88,90}Mo were obtained in three experiments, performed at the VICKSI acceler-

*Present address: Physics Division, Oak Ridge National Laboratory, Oak Ridge, TN 37831.

ator at the Hahn-Meitner-Institut in Berlin and at the Van de Graaff tandem accelerator in Cologne. In two of these measurements, the heavy ion fusion evaporation reaction ^{58}Ni(^{36}Ar, $xpynz\alpha$) with the pulsed ^{36}Ar beam of the VICKSI facility was used at beam energy 149 MeV and 140 MeV to obtain Doppler-broadened line shapes, directional correlations of oriented states (DCO's), and lifetimes via recoil distance methods. A singles angular distribution experiment in Cologne provided additional information on multipole mixing ratios and alignments of ^{90}Mo states. The reaction ^{58}Ni(^{35}Cl,$xpynz\alpha$), at 120 MeV beam energy, was used for this measurement.

A. Determination of mixing ratios

The ^{58}Ni + ^{36}Ar experiment has been described previously [5,7], and therefore, only information relevant for the present study is given here. The measurement was carried out with a 149-MeV pulsed ^{36}Ar beam which bombarded a 99.8% enriched, 19.8 mg/cm^2 thick ^{58}Ni target foil. The residual nuclei ^{88}Mo and ^{90}Mo were produced in the $\alpha 2p$ and $4p$ evaporation channels from the compound nucleus ^{94}Pd. The experimental relative yield of ^{88}Mo was estimated to be 13.5(5)% and that of ^{90}Mo to 30.4(9)% of the total fusion evaporation cross section. The resulting γ radiation was measured by the OSIRIS spectrometer [20], consisting of 12 BGO shielded Ge detectors of 25–30% efficiency which were mounted in two rings at 65° and 115° to the beam direction. The $\gamma\gamma$ correlation analysis was enabled by the additional high purity Ge detector at 162°. This detector has been also used to obtain Doppler broadened line shapes of prompt transitions.

The $\gamma\gamma$ correlations from oriented nuclear states provide information on the multipolarities of electromagnetic transitions. This was used in previous work to make spin parity assignments to residual nuclei from the ^{58}Ni + ^{36}Ar reaction [1,5–7,9,10]. In the OSIRIS geometry, the experimental DCO ratio is defined as

$$R_{\mathrm{DCO}} := \frac{I(\gamma_1 \text{ at } 162^\circ \text{ ; gated with } \gamma_2 \text{ at } 65^\circ, 115^\circ)}{I(\gamma_1 \text{ at } 65^\circ, 115^\circ \text{ ; gated with } \gamma_2 \text{ at } 162^\circ)}, \quad (1)$$

where I denotes the relative coincidence intensity. The comparison between the experimental R_{DCO} values and

TABLE I. Summary of singles angular distributions and angular correlations data for ^{90}Mo.

I_i^π [$\hbar$] $\rightarrow$ I_f^π [$\hbar$]	E_γ [keV]	A_2	A_4	δ_{SAD}	R_{DCO}	δ_{DCO}	$\bar{\delta}$
$22^+ \rightarrow 21^+$	280.2	-0.41(3)	0.06(3)	0.10(8)	0.40(8)	$0.15\binom{14}{10}$	$0.12\binom{8}{6}$
$21^+ \rightarrow 20^+_2$	620.5	-0.53(5)	0.13(6)	0.16(13)	0.38(11)	0.16(12)	0.16(9)
$20^+_2 \rightarrow 18^+$	1709.9	0.37(3)	-0.03(4)		1.18(10)		
$\rightarrow 19^+$	495.7	-0.46(8)	0.03(1)	0.14(23)	0.70(6)[a]	-0.1	0.14(23)
$19^- \rightarrow 17^-$	1804.0	0.34(6)	-0.02(6)		0.91(8)		
$18^+ \rightarrow 16^+$	1779.2	0.33(4)	-0.05(4)		1.05(11)		
$17^- \rightarrow 15^-$	872.0	0.29(2)	-0.05(2)		1.03(6)		
$\rightarrow 16^+$	768.9	-0.19(2)	0.07(2)	-0.02(6)	0.60(7)	$0.02\binom{9}{7}$	0.00(5)
$\rightarrow 16^-$	129.4	-0.38(4)	-0.00(5)	0.14(14)	0.24(8)[b]		0.14(14)
$16^- \rightarrow 15^-$	742.5	-0.56(3)	0.24(3)	3.1(8)	0.69(7)[c]		3.1(8)
$16^+ \rightarrow 15^+$	598.0	-0.53(2)	0.16(2)	3.1(4)	0.56(6)	4.6(16)	3.4(5)
$15^- \rightarrow 14^+_1$	1018.1	-0.23(2)	0.03(3)	-0.01(6)	0.65(7)	$-0.06\binom{7}{5}$	-0.04(4)
$\rightarrow 13^-$	943.5	0.33(2)	0.04(2)		0.97(7)		
$14^- \rightarrow 13^-$	776.2	-0.69(6)	0.34(7)	2.7(10)	0.51(8)	$3.6\binom{17}{11}$	$3.1\binom{10}{7}$
$15^+ \rightarrow 14^+_1$	523.2	-0.45(1)	0.05(1)	0.13(3)	0.50(6)	$0.06\binom{8}{5}$	0.11(3)
$\rightarrow 14^+_2$	244.5	-0.45(2)	0.07(2)	0.12(3)	0.43(7)[b]	(0.13)	0.12(3)
$14^+_2 \rightarrow 13^-$	526.5	-0.45(2)	0.05(3)	0.13(6)	0.42(7)	0.14(7)	0.13(5)
$13^- \rightarrow 12^+$	1143.8	-0.28(2)	0.03(2)	0.02(5)	0.66(8)	$-0.07\binom{7}{6}$	-0.02(4)
$\rightarrow 11^-$	857.7	0.34(2)	-0.09(2)		0.94(5)		
$14^+_1 \rightarrow 12^+$	1069.1	0.35(2)	-0.11(3)		0.91(7)		
$\rightarrow 13^+$	247.8	-0.30(2)	0.02(2)	0.04(5)	0.36(7)[b]	(0.19)	0.04(5)
$13^+ \rightarrow 12^+$	821.4	-0.41(1)	0.05(2)	0.10(4)	0.49(6)	0.07(8)	0.09(4)
$11^- \rightarrow 10^+_2$	649.6	-0.34(3)	0.06(3)	0.04(6)	0.66(8)	-0.06(7)	-0.01(5)
$\rightarrow 9^-$	544.2	0.1(2)[d]	0.0(2)[d]		1.01(6)		
$9^- \rightarrow 9^-$	296.5	0.44(3)	-0.03(3)	$-0.2\binom{4}{3}$			$-0.2\binom{4}{3}$
$12^+ \rightarrow 10^+_1$	477.0	0.33(1)	-0.09(2)		1.01(6)		
$\rightarrow 10^+_2$	363.3	0.22(2)[e]	-0.06(2)[e]		0.95(9)		
$10^+_2 \rightarrow 8^+_1$	1317.7	0.31(1)	-0.06(2)		1.00(8)		
$10^+_1 \rightarrow 8^+_2$	972.7	0.32(1)	-0.08(2)		0.99(9)		
$7^- \rightarrow 5^-$	818.6	0.26(2)	-0.00(2)		0.99(6)		
$8^+_2 \rightarrow 8^+_1$	231.4	0.38(1)	-0.01(2)	$-0.04\binom{10}{40}$	0.71(7)[b]		$-0.04\binom{10}{40}$
$5^- \rightarrow 4^+$	546.7	-0.20(2)	0.00(2)	0.01(6)	0.60(6)	$0.03\binom{10}{8}$	$0.02\binom{8}{5}$

[a]DCO ratio most probably overestimated due to Doppler-broadened lineshape.
[b]DCO ratio underestimated due to different timing properties of the 162° detector and the OSIRIS ring (see Refs. [7,21] for details).
[c]DCO ratio too large due to contamination with β^+ activity in the $\gamma\gamma$ matrix.
[d]In the singles spectra, the line is contaminated with β^+ activity.
[e]Doublet structure.

their theoretical predictions via the multipole mixing ratio δ was used to evaluate the multipole character of transitions in ^{88,90}Mo. In geometries with nearly cylindrical symmetry, the method described in a recent paper by Kabadiyski, Lieb, and Rudolph [21] also provides the possibility to determine $\delta(E2/M1)$ mixing ratios of transitions with $\Delta I = 0, 1$. The phase convention of Rose and Brink [22] was used. The results of the DCO analysis for ^{90}Mo are summarized in Table I. As discussed in Ref. [21], the method provides two possible solutions for δ which also depend on the alignment attenuation coefficients α_2 of the initial states. If only one pair of angles is used, one of the two solutions can be eliminated only via comparison with nuclear model predictions or singles angular distribution measurements. An additional singles angular distribution experiment, with a 99.8% enriched 16.3 mg/cm^2 thick ^{58}Ni target, was carried out to distinguish between the two solutions for ^{90}Mo transitions.

The reaction ^{58}Ni(^{35}Cl, $3p$)^{90}Mo at the Van de Graaff tandem accelerator in Cologne was used to obtain angular distribution data for positive parity states above the yrast 8^+ isomeric state ($T_{1/2} = 1.05$ μs) and for most of the yrast negative parity states. The setup of this experiment has been described in a recent work by Rudolph *et al.* [9]. Four Ge detectors of 25–55% relative efficiency were used to detect the γ radiation, one of them being positioned at 125° to the beam to monitor the beam current. The other three detectors were mounted at angles of 55° and 45°, relative to each other and scanned the region from −90° to +10° relative to the beam direction.

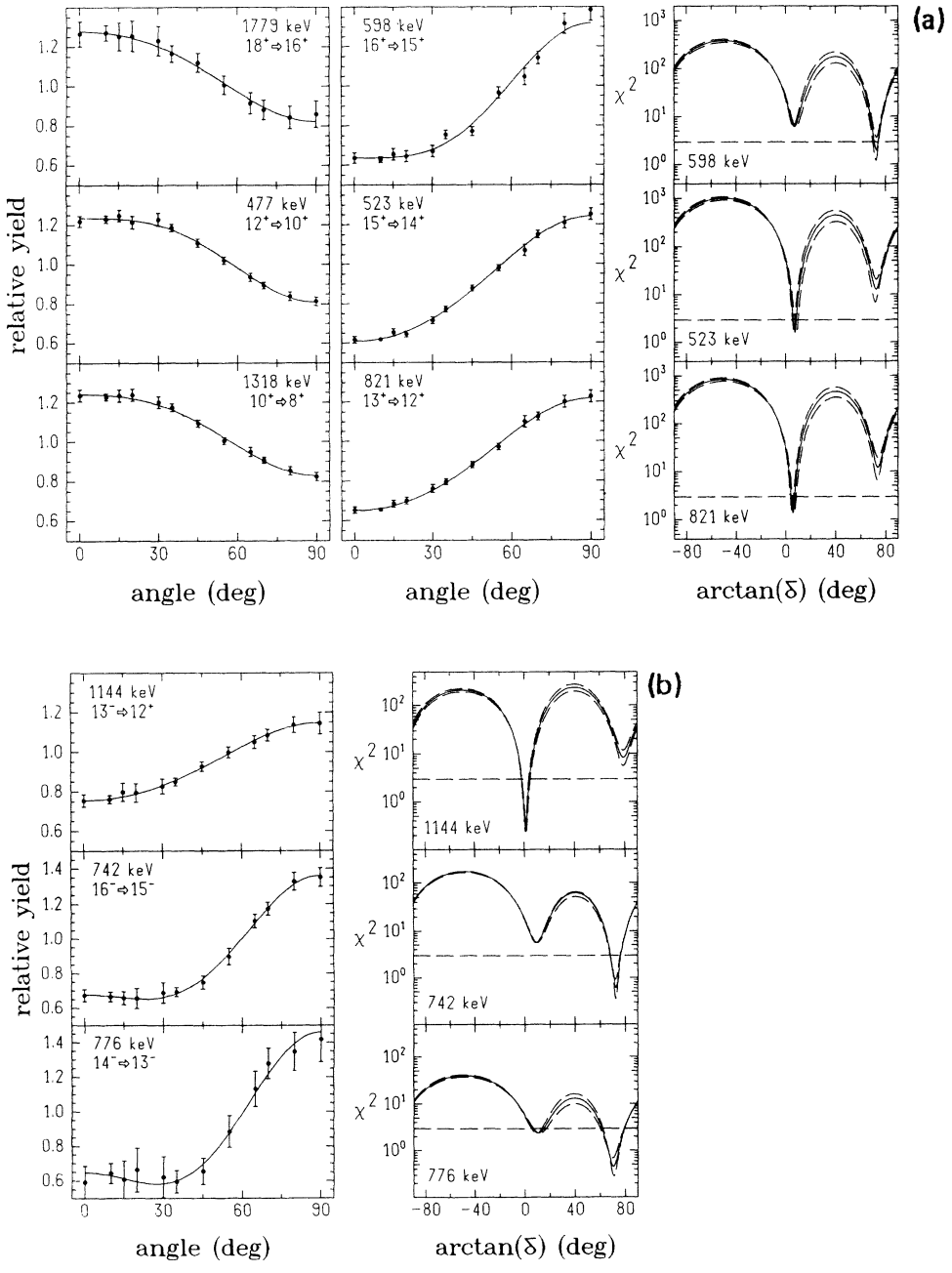

FIG. 1. Angular distributions and χ^2 analysis of mixing ratios for $\Delta I = 1$ transitions in ^{90}Mo for (a) positive parity states and (b) negative parity states. The experimental relative yields were fitted with Legendre polynomials according to formula (2). The solid curves in the χ^2 plots correspond to the analysis with the best values for the alignment coefficients α_2. The dashed ones represent calculations with the upper and lower limits of α_2.

Making use of the symmetry characteristics of angular distributions, the relative yields of the γ radiations were obtained at 12 different angles between 0° and 90°. The left and middle parts of Fig. 1(a) and the left part of Fig. 1(b) show examples of least-squares fits to the data using the Legendre polynomial formula [23]

$$W(\theta) = A_0 + A_2 P_2(\cos\theta) + A_4 P_4(\cos\theta). \quad (2)$$

The A_2 and A_4 values listed in Table I are the fitted numbers corrected for the attenuation due to the finite solid angles of the Ge detectors [24,25]. The A_2 and A_4 coefficients depend on the alignment attenuation coefficients α_k and the multipole mixing ratio δ between the amplitudes of the two lowest multipoles [23]. The coefficients α_k are defined by $\alpha_k := A_k^{\rm expt}/A_k^{\rm max}$ $(k = 2, 4)$ where $A_k^{\rm max}$ denotes the theoretical value for complete alignment at the same δ value. Furthermore, under the assumption of the Gaussian distribution of magnetic substates which is appropriate for heavy ion fusion reactions, there is a functional correlation between α_2 and α_4 [23,26]. Therefore, the measurement of $A_2^{\rm expt}$ and $A_4^{\rm expt}$ should be sufficient to obtain the three variables α_2, α_4, and δ. Because of the statistical uncertainties of $A_2^{\rm expt}$ and $A_4^{\rm expt}$, this procedure results in a χ^2 analysis to the experimental yields [27]. This is illustrated in the right part of Fig. 1 for several $\Delta I = 1$ transitions in ^{90}Mo. The solid curves correspond to the analysis with the best values for α_2. Dashed lines represent their upper and lower limits. The resulting mixing ratios given in Table I refer to the absolute minima of the solid curves and the errors correspond to the largest interval between adjacent crossing points of the three curves and the 0.1% confidence limit. It should be noted that several $\Delta I = 1$ transitions in ^{90}Mo were found to have large δ values. These are the 598 $(16^+ \rightarrow 15^+)$, the 742 $(16^- \rightarrow 15^-)$ keV, and the 776 keV $(14^- \rightarrow 13^-)$ lines (see Fig. 1). We suggest different physical reasons responsible for this effect, as will be discussed in more detail later in this work. It is worthwhile noting that all earlier proposed parity changing transitions in ^{90}Mo [7,16] have δ values consistent with zero, in agreement with an $E1$ character.

The α_2 coefficients for ^{90}Mo obtained from the angular distribution measurement were compared with values from Monte Carlo simulations of the magnetic substate populations of the same states in the ^{58}Ni+^{36}Ar reaction which should result in a similar magnetic substate population. The calculations were performed with the code GAMMAPACE [28]. Very good agreement between theoretical and experimental values was obtained. Instructive results include the agreement for the yrast 12^+ state with an experimental alignment of $\alpha_2 = 0.80(3)$ and corresponding theoretical value of 0.82; the yrast 10^+ state with 0.77(3) from the experiment, 0.78 from theory; and the yrast 5^- state with 0.61(5) from the experiment, 0.64 from theory . This agreement leads to the conclusion that due to the large number of deexcitation cascades, the attenuation coefficients α_2 have values which closely follow those of the direct population.

Therefore, we used the same method to calculate the alignments of the ^{88}Mo states and thus to calibrate the DCO analysis of the nucleus. The DCO ratios presented in Ref. [5] have been further used to obtain mixing ratios. The resulting α_2 and δ values for ^{88}Mo are presented in Table II. Figure 2 presents the DCO analysis of the 359 keV $(19^- \rightarrow 18^-)$ and the 272 keV $\Delta I = 0$ transitions.

TABLE II. Multipole mixing ratios for mixed dipole-quadrupole transitions in ^{88}Mo obtained from angular correlations.

I_i^π [$\hbar$]	I_f^π [$\hbar$]	E_γ [keV]	α_2[a]	$R_{\rm DCO}$	$\delta_{\rm DCO}$	
21^-	20^-	374.6	0.93	0.49(3)	0.05(3)	4.0(4)
20^-	19^-	492.8	0.92	0.53(6)	0.02(5)	$4.6\binom{13}{9}$
19^-	18^-	727.1	0.91	0.33(11)	$0.21\binom{14}{11}$	$2.4\binom{9}{7}$
19^-	18^-	358.6	0.91	0.42(7)	0.12(6)	$3.1\binom{8}{6}$
18^-	17^-	761.0	0.90	0.56(3)	0.0(3)	$5.0\binom{7}{5}$
17^-	17^-	419.0	0.89	0.77(16)	$-1.0\binom{3}{5}$	0.7(3)
18^+	17^+	361.7	0.90	0.55(5)	0.01(4)	$4.8\binom{11}{8}$
17^+	16^+	820.4	0.89	0.59(7)	-0.02(6)	$5.6\binom{24}{13}$
16^+	15^+	398.5	0.88	0.46(17)	$0.09\binom{18}{14}$	$3.5\binom{33}{14}$
16^+	15^+	395.2	0.88	0.57(5)	0.00(4)	$5.2\binom{13}{9}$
15^+	14^+	590.2	0.86	0.51(3)	0.05(3)	4.0(4)
14^+	14^+	247.7	0.85	0.87(12)[c]	$\lvert\delta\rvert < 0.7$	
10^+	10^+	253.0	0.79	1.01(12)[c]	$\lvert\delta\rvert < 0.5$	
10^+	10^+	163.0	0.79	0.67(7)[c]	$\lvert\delta\rvert < 1.1$	
8^+	8^+	271.7	0.75	0.88(6)[c]	$\lvert\delta\rvert < 0.6$	
7^-	6^+	723.0	0.72	0.65(11)[b]	-0.06(9)[b]	

[a] α_2 calculated from Monte Carlo simulations of the direct level feeding (see Refs. [21,28]) for details.
[b] The $M2/E1$ mixing ratios for $E1$ transitions are calculated to check consistency of the spin-parity assignments.
[c] DCO ratio underestimated due to different timing properies of the 162° detector and the OSIRIS ring (see Refs. [7,21]) for details.

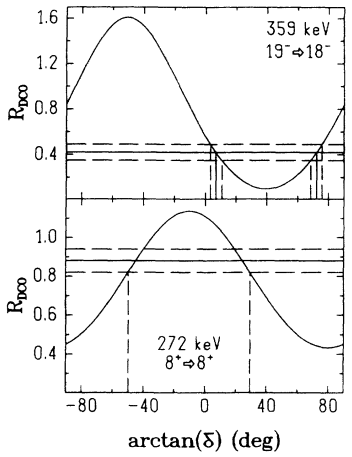

FIG. 2. Illustrative DCO analysis of $\Delta I = 1$ and $\Delta I = 0$ transitions in ^{88}Mo. Vertical solid lines represent the two multipole mixing ratio solutions which are obtained from the crossings of the theoretical DCO curves and the experimental value (horizontal lines). Dashed lines indicate corresponding uncertainties.

For $\Delta I = 0$ transitions, only upper limits for $|\delta|$ are given (see lower part of Fig. 2) due to their low energies which caused timing problems (for details see Refs. [7,21]).

B. Lifetimes

The ^{58}Ni+^{36}Ar experiment also gave information on lifetimes via Doppler-shift attenuation line shape analysis (DSA). Transitions between yrast states above 16^+ and 17^- in ^{90}Mo were found to have discernible DSA line shapes from which lifetimes could be deduced. No transitions in ^{88}Mo could be evaluated for lifetimes via DSA because of insufficient coincidence statistics. Extensive calculations with the Monte Carlo code TRIM [29] were performed to simulate the velocity distribution of the ^{36}Ar projectiles and the recoiling ^{90}Mo nuclei in the thick ^{58}Ni target. Additional calculations with the fusion evaporation code PACE [30] resulted in an active target depth of 3 mg/cm^2 accounting for the production of ^{90}Mo recoils. The distributions of initial velocities and relative reaction cross sections obtained from PACE were then incorporated into TRIM calculations to simulate the slowing down process in 30 target layers of 100 μg/cm^2 thickness each. The calculations yielded a relatively narrow velocity spread of the ^{90}Mo recoils in the first layer arround the mean value $v/c = 0.0377$ while a broad velocity distribution between $v_{\min}/c = 0.0133$ and $v_{\max}/c = 0.0324$ with a large directional spread was found for the 30th layer. This extensive information was used with the Monte Carlo line shape evaluating code LILIFI [31] to obtain a slow-down history for 10^4 ^{90}Mo recoils. The Doppler-broadened line shapes of the 280-, 459-, 496-, 621-, 881-, 1779-, and 1919-keV transitions were analyzed in this fashion. The solid cascade feeding pattern for each transition was taken from [7]. Where necessary, effective side feeding times were also fitted as free parameters. In all such cases, the effective side feeding was found to vary in the range 50–100 fs. The fit to the 459-keV $18^+ \rightarrow 17^+$ line in ^{90}Mo which is illustrated in Fig. 3 includes the cascade feeding of the 1710-keV transition. The unknown lifetimes of the weak 919-, 1263-, and 1214-keV feeders were incorporated in an effective side feeding which was simultaneously fitted with the main transition. The calculations yielded a narrow χ^2 minimum at $\tau_{\text{mean}} = 0.24(6)$ ps and $\tau_{\text{sf}} = 0.6(1)$ ps. For the lifetime of the 881-keV transition, only an upper limit was obtained due to the unknown feeding pattern. Mean lifetimes via DSA were calculated for all other transitions mentioned above. The corresponding values are presented in Table III. The excellent overlap between the two values for the mean lifetime of the 8525-keV level is worth noting. However, no transitions above spin 17^- in ^{90}Mo could be fitted due to insufficient statistics.

The fact that transitions between levels in the intermediate and low spin regions in ^{88,90}Mo do not show any Doppler broadening indicates mean lifetimes longer than 2 ps or long-lived feeder states. Therefore, we performed a recoil distance experiment with the same reaction at the VICKSI accelerator in Berlin using a plunger apparatus designed by Dewald *et al.* [32]. The 140-MeV ^{36}Ar beam bombarded a 1.25-mg/cm^2 stretched self-supporting ^{58}Ni foil enriched to 99.8%. The stopper was a stretched 7 μm thick gold foil which permitted flight distances between 3.5 μm and 10 000 μm. In addition to the singles spectra, $\gamma\gamma$-coincidence events were recorded at flight distances of 3.5 μm, 50 μm, 100 μm, and 200 μm. An extensive description of the setup and data reduction can be found in recent work by Rudolph *et al.* [10]. The mean velocity of the recoiling ^{88}Mo nuclei was $v/c = 0.0278(1)$, and the ^{90}Mo nuclei recoiled at a $v/c = 0.0269(1)$. These values were obtained by the exact Doppler-shift formula applied to the flight and stopped peaks at 0° after correction for shift attenuation due to the finite solid angle of the 0° detector:

$$\beta = \frac{\left(1 + \frac{2\beta^{(1)}}{1+\cos\theta_c}\right)^2 - 1}{\left(1 + \frac{2\beta^{(1)}}{1+\cos\theta_c}\right)^2 + 1}. \tag{3}$$

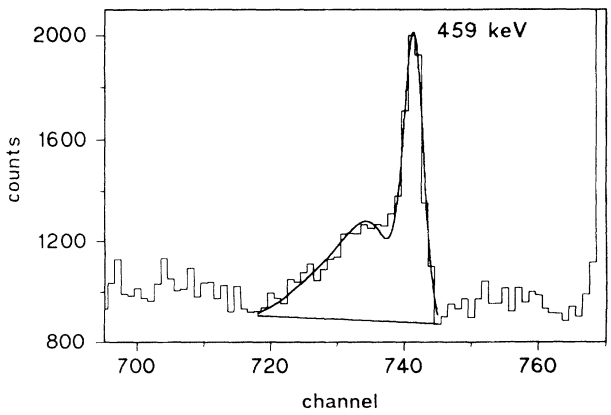

FIG. 3. Doppler-broadened line shape of the 459 keV $18^+ \rightarrow 17^+$ transition in ^{90}Mo measured at 162°. The solid curve represents the best fit with the code LILIFI [31].

Here, $\beta^{(1)}$ denotes the relative recoil velocity, as obtained from the experimental flight peak by the first-order Doppler-shift formula, and θ_c is the maximum angle, subtended by the detector. Equation (3) implies a uniform angular distribution of the γ rays within the narrow solid angle of the shielded 0° detector and a constant detector response which leads to the shift attenuation factor $(1+\cos\theta_c)/2$ [33].

The decay functions of stopped components in ^{90}Mo and ^{88}Mo, some of which are presented in the left-hand parts of Figs. 4 and 5, were analyzed by the recoil distance Doppler-shift method (RDDS) using the program CRONOS [34]. As can be seen from Fig. 4, the yrast 12^+ state in ^{90}Mo which is deexcited by the 363- and 477-keV transitions is isomeric. A mean lifetime of 759(5) ps was obtained for this state (see Table III). This is in agreement with the subnanosecond character of the state first reported by Arnell *et al.* [16], although these authors deduce a somewhat lower value of 0.4(1) ns. Special attention was paid to resolving doublets, since they can contribute significantly to the feeding uncertainty for lower lying transitions in the same cascades. The least-squares fit procedure used allows the unfolding of decay functions with significantly differing lifetimes. Such an example is presented in Fig. 5 with the 972-keV $6^+ \rightarrow 4^+$ transition in ^{88}Mo. It is an energetically unresolved doublet with the $10_1^+ \rightarrow 8_2^+$ transition in ^{90}Mo. However, the ratio of the two effective lifetimes is 1:17.4 due to the isomeric nature of the 12^+ state in ^{90}Mo. As illustrated, the long-lived component of the doublet is resolved by fitting an independent single exponent to the observed decay function.

In addition to the common RDDS analysis, the data were also analyzed via the differential decay curve method (DDCM) introduced by Dewald *et al.* [35] and Böhm *et al.* [36]. In our case, the use of extrapolated decay function values at zero distance was avoided by taking the ratios of the efficiency corrected areas of the

TABLE III. Lifetimes in ^{90}Mo.

E_x [keV]	E_γ [keV]	RDDS τ [ps]			DDCM τ [ps]			DSA τ [ps]	$\overline{\tau}$ [ps]
		0°	42°	138°	0°	42°	138°		
12016.6	880.8		1.5(4)[a]					1.4(6)[a]	< 1.8
11135.9	280.2							< 0.1	< 0.1
10855.7	620.5							1.3(2)	1.3(2)
10235.2	495.7							0.30(8)	0.30(8)
8525.4	1779.2							0.23(4)	0.23(3)
	458.6							0.24(6)	
8066.8	1918.6							0.87(5)	0.87(6)
	1320.8		$0.8\binom{6}{3}$			0.9(6)			
7515.1	872.0	10.5(7)	11.2(14)	11.1(3)	10.5(2)	11.4(5)	11.0(1)		10.7(5)
	768.9	11(3)	11(1)	7.8(6)	11.3(3)	10.8(1)	7.8(1)		
	129.4		(13.5)						
7385.6	742.5		10(3)	9(3)					9.5(22)
6746.2	598.0								5.2(10)[b]
6643.1	1018.1		$1.4\binom{24}{9}$	$1.6\binom{22}{8}$		2.1(2)	1.8(2)		1.9(2)
	167.1			$1.7\binom{12}{4}$					
6475.8	776.2			2.2(14)					2.2(14)
6148.2	523.2[c]								< 0.4
	244.5		$0.2\binom{3}{2}$	$0.2\binom{3}{2}$		0.1(2)	0.13(8)		
5903.7	526.5			2.4(6)			2.3(3)		2.4(6)
5699.6	1143.8		2.1(9)	1.9(7)		2.2(4)	2.0(2)		2.0(6)
5625.0	247.8	4.0(3)	4.1(4)	3.7(4)	4.1(4)	3.9(5)	4.3(2)		3.9(2)
5377.2	821.4		1.4(9)	1.5(6)					1.4(5)
4842.0	649.6			53(6)			53(2)		56(3)
	544.2		57.3(14)	54(13)		58.9(7)	51(5)		
4555.8	477.0	780(8)	752(4)	740(5)	783(5)	755(4)	734(3)		759(5)
	363.3	762(20)	759(6)	761(6)			764(5)		
4297.7	930.3			14(3)					14(3)
4192.5	1317.7	< 5	< 5	< 5					< 5
4079.0	972.7	23(7)	21(7)	$17\binom{9}{8}$					21(4)
3367.4	818.6	< 0.4		< 1.6					< 1
	555.7			< 0.6					
3106.3	231.4	7(4)	8(4)	6(4)			10(6)		7(2)
2548.8	546.7		23(4)						23(4)

[a]Effective lifetime.
[b]The decay function was taken from the $\gamma\gamma$ matrices.
[c]The sum of all decay curves was analyzed.

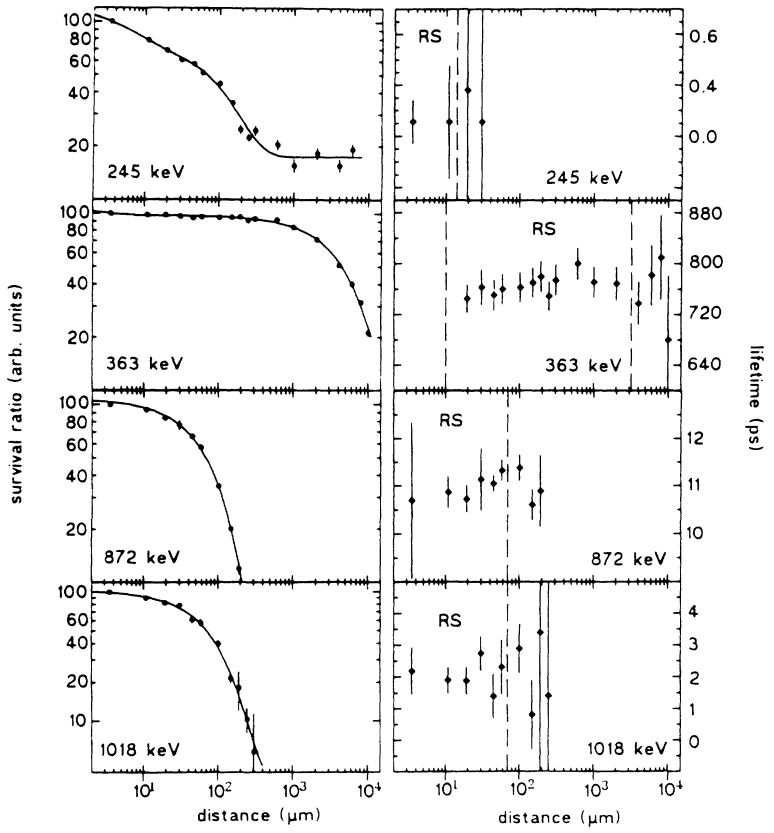

FIG. 4. Recoil distance survival ratios (left-hand side) and corresponding lifetimes from the DDCM analysis (right-hand side) of transitions in ^{90}Mo. For each decay curve, RS denotes the region of sensitivity (see Ref. [35] for details).

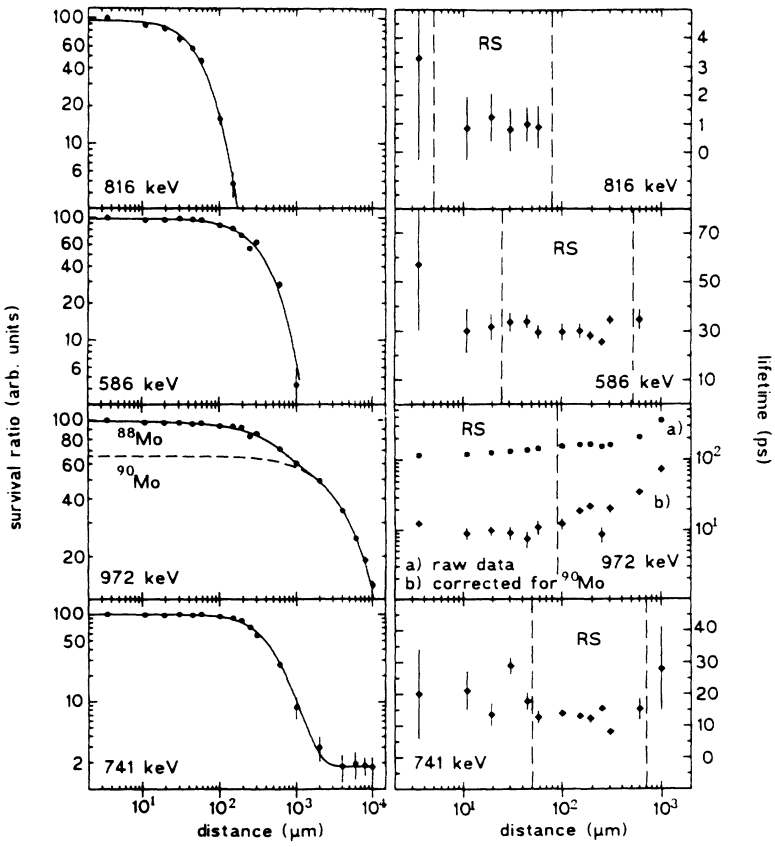

FIG. 5. Recoil distance survival ratios (left-hand side) and corresponding lifetimes from the DDCM analysis (right-hand part) of transitions in ^{88}Mo. For each decay curve, RS denotes the region of sensitivity (for details see Ref. [35]). Where possible, doublets were differentially analyzed which contain significantly differing lifetimes (for explanations see text).

direct feeder and main transition stopped components at the lowest distance and also normalizing the decay functions to this distance. The stopped component areas for the direct feeders at lowest distance were taken from the spectra or were simulated with effective lifetimes. The first derivatives of the normalized decay functions were either calculated from the experimental relative yields or obtained from the RDDS fit curve if it covered all points. The background intensity was taken from the RDDS fit. In cases when all parameters for the direct feeders could be taken from experimental decay functions, the two analyses were assumed to give sufficiently independent values for the level mean lifetime. In all other cases, the mean values given at the right-hand side of Tables III and IV reflect the mean of RDDS (and DSA) data. The right-hand sides of Figs. 4 and 5 illustrate the results of the DDCM analysis for the same transitions shown at the left-hand side. RS denotes the region of sensitivity defined in Ref. [35]. The complex nature of the decay function of the 972-keV line can also be seen in the DDCM analysis. The *raw* decay function leads to a lifetime steadily increasing with distance, while the subtraction of an exponent with the lifetime of the isomeric contaminant leads to much smaller and nearly constant lifetime values within the region of sensitivity.

III. COMPARISON OF ELECTROMAGNETIC PROPERTIES OF STATES IN ^{88}Mo AND ^{90}Mo

The extensive data set presented in Sec. II offers the possibility for a detailed analysis of the electromagnetic properties of high spin states in the neutron-deficient even molybdenum isotopes near the onset of collectivity. In a recent work on the systematic behavior of these nuclides [2], Gross *et al.* propose a rather smooth transition from near spherical to deformed nuclear shapes at $N = 46$ which is in contradiction with the drastic variation predicted by Möller and Nix [37]. The well-known dramatic influence of single nucleons on the collective behavior of excited nuclear states in this mass region still leaves many questions open. Here we mention the abrupt increase of collectivity in ^{87}Mo [3] when going from the $(1qp)$ $g_{9/2}$ band to the $(3qp)$ band. On the other hand, Weiszflog *et al.* [5] have worked out a surprisingly simple seniority classification scheme of the excited states in ^{88}Mo within a shell model approach considering valence particles and holes in the restricted configuration space $\pi(2p_{1/2}, 1g_{9/2})\nu(2p_{1/2}, 1g_{9/2})$. In addition, high spin excitations in ^{90}Mo can be explained mainly in the same shell model configuration space [7] despite the apparent need of a larger model space which was indicated by cal-

TABLE IV. Lifetimes in ^{88}Mo.

E_x [keV]	E_γ [keV]	RDDS τ [ps]			DDCM τ [ps]			$\bar{\tau}$ [a] [ps]
		0°	42°	138°	0°	42°	138°	
8609.4	761.0							< 0.7[b]
8127.4	361.7							< 0.5[b]
7848.4	980.1	1.7(4)	1.8(3)		1.7(1)	1.8(3)		1.8(1)
7322.9	1115.8		0.4(3)[c]			0.44(6)[c]		< 0.5
6944.8	395.2							< 0.9[b]
6868.2	898.5		4.1(3)	6.2(3)				5.1(3)[d]
6549.5	590.2		0.6(3)			0.7(2)		0.7(2)
6207.0	934.6		2.5(18)	2.3(4)		2.7(2)	2.6(2)	2.6(2)
5969.7	816.3	1.1(7)	1.2(6)	1.4(6)	1.0(3)	1.4(5)	1.5(5)	1.3(2)
5959.3	906.8	9(1)	8.4(3)	7.8(4)	8.5(3)	8.5(1)	7.7(1)	8.18(8)
5272.4	1077.2			0.8(3)			0.7(2)	0.8(2)
5153.4	839.6	1.5(9)		2.3(9)	1.7(5)		1.8(12)	1.8(4)
5052.5	857.3			27(3)			25(2)	26(2)[e,f]
4313.8	964.0		3.6(12)	3.7(10)			3.8(5)	3.7(5)
4195.2	982.3	6.9(8)	7.8(9)	6.4(3)	6.3(4)	6.1(3)	5.9(2)	6.3(1)
3484.7	271.7		4.5(6)[c]	4.9(6)[c]				< 5.1
3349.8	703.4		6.9(10)	6.7(10)		5.6(3)	7.5(5)	6.7(8)
3213.0	586.1	33.7(9)	32.8(9)	28(2)	36(4)	33(1)	30.3(8)	32.0(5)
2646.4	991.6		$19\binom{7}{4}$	$19\binom{7}{3}$		20.0(5)	19.8(5)	19.8(4)
2626.9	971.9	10(2)	13(2)	17(3)	10(1)	10.2(7)	13.2(9)	11.6(5)[f]
1654.9	914.3					1.3(2)	1.4(2)	1.4(2)
740.6	740.6	9.6(9)	8.5(5)	10.6(7)		10.4(4)	12.4(5)	10.3(3)

[a] All upper limits mean the measured effective lifetime plus one standard deviation.
[b] The decay function was taken from the $\gamma\gamma$ matrices.
[c] Effective lifetime.
[d] Fitted also as feeder of the 5970-keV level at 0° and 138° (for details see text).
[e] Fitted also as feeder of the 4195-keV level.
[f] Fitted with an additional independent exponent due to doublet structure.

culations in the isotone ^{88}Zr [38,39]. On the other hand we find a large number of stretched $E2$ transitions with similar energies on both parity sides in ^{88}Mo which may exhibit a vibrational structure.

In the following, we investigate some of these problems by comparing the measured electromagnetic decay properties of states in ^{88}Mo and ^{90}Mo listed in Tables V and VI. Due to the presence of the interconnecting $E1$ transitions in both nuclides, we have followed a notation for the multipole strengths which is related to the lowest multipole σL. For each transition, the latter is indicated explicitly in column 4 of the tables. The discussion of the $B(\sigma L)$ shell model predictions in ^{90}Mo with two different residual interactions, also presented in Table VI, is given in Sec. IV.

A. Positive parity states

Before the present experiments, the question about the degree of collectivity of ^{88}Mo had not been answered. The deduced $B(E2, 2^+ \rightarrow 0^+)$ strength of 15.3(4) W.u. (see Table V) is only half the value of the semiempirical estimation of Weiszflog *et al.* [5], which yields $|\beta_2| = 0.13$ in the axial rotor limit. A recent consistent set of Hartree-Fock-Bogolyubov calculations on nuclear deformation parameters in this region [40] predicts $|\beta_2| = 0.10$ for ^{88}Mo in good agreement with the above value. We suggest that, in its ground state, ^{88}Mo sustains a nearly spherical shape which may perform quadrupole vibrations. The energy ratio of the lowest $2^+$and 4^+ states, $E(4^+)/E(2^+) = 2.23$, is additional support for vibrations as well as the enhanced $B(E2; 4^+ \rightarrow 2^+)$ value of 40(5) W.u. The lowering of the 2_1^+, 0_2^+, 2_2^+, and 4_1^+ states has already been observed in earlier works on the neighboring isotope ^{90}Mo [17,41], the $(0_2^+, 2_2^+, 4_1^+)$ triplet being interpreted as a two-phonon triplet. Unfortunately, the 8_1^+ isomeric state prevents the direct measurement of the quadrupole transition strengths in the ground state band of ^{90}Mo via conventional RDDS and so no direct evidence for the corresponding $E2$ strengths is available. A coupling between two neutron holes or proton particle excitations to the vibrational motion is most probably responsible for the enhanced $B(E2)$ strengths of the $4_1^+ \rightarrow 2_1^+$ and $8_1^+ \rightarrow 6_1^+$ transitions in ^{88}Mo (see Table V) while the $6_1^+ \rightarrow 4^+$ transition shows a surprisingly low quadrupole strength.

The $E2$ transitions in the intermediate and high spin positive parity region of ^{88}Mo have in general larger $B(E2)$ values than the corresponding transitions in ^{90}Mo. The $v = 4, 6$ positive parity states in ^{88}Mo have most probably a highly mixed structure. A second short-lived 12^+ state [$\tau = 0.76(15)$ ps] is observed which deexcites to the two 10^+ states with $E2$ strengths between 20 and 30 W.u. The lowering of the energy of the 14_1^+ level prevents the population of a 13^+ state which lies higher in

TABLE V. Reduced transition probabilities in ^{88}Mo. σL denotes the lowest multipole which is visible via γ radiation. For mixed transitions, $\tilde{\sigma} L + 1$ denotes the next higher multipole.

E_x	$I_i^\pi \rightarrow I_f^\pi$		Positive parity states [a,b]		E_x	$I_i^\pi \rightarrow I_f^\pi$		Negative parity states [a]	
[keV]	[$\hbar$]	σL	$B(\sigma L)\downarrow$	$B(\tilde{\sigma} L{+}1)\downarrow$	[keV]	[$\hbar$]	σL	$B(\sigma L)\downarrow$	
8127.4	$18_1^+ \rightarrow 16_1^+$	$E2$	> 309		8609.4	$18_1^- \rightarrow 17_1^-$	$M1$	> 0.18[c]
	$\rightarrow 17_1^+$	$M1$	> 1.3[c]		7848.4	$17_1^- \rightarrow 15_1^-$	$E2$	516(33)
7322.9	$16_3^+ \rightarrow 14_2^+$	$E2$	> 944		6868.2	$15_1^- \rightarrow 13_1^-$	$E2$	273(16)
6944.8[d]	$16_1^+ \rightarrow 15_1^+$	$M1$	> 1[c]		5969.7	$13_1^- \rightarrow 11_1^-$	$E2$	$1.8\binom{3}{2} \times 10^3$
6549.5	$15_1^+ \rightarrow 14_1^+$	$M1$	$0.38\binom{13}{8}$	$39\binom{23}{15}$	5153.4	$11_1^- \rightarrow 9_1^-$	$E2$	$1.0\binom{3}{2} \times 10^3$
	$\rightarrow 14_2^+$	$M1$	$0.20\binom{7}{4}$[c]			$\rightarrow 9_2^-$	$E2$	$415\binom{117}{76}$
6207.0	$14_2^+ \rightarrow 12_1^+$	$E2$	28(2)		4313.8	$9_1^- \rightarrow 7_1^-$	$E2$	$257\binom{36}{28}$
	$\rightarrow 12_2^+$	$E2$	298(20)			$\rightarrow 8_1^+$	$E1$	$3.2\binom{7}{4} \times 10^{-6}$
	$\rightarrow 14_1^+$	$M1$	> 0.14[e]	$< 1.65 \times 10^4$ [e]	3349.8	$7_1^- \rightarrow 5_1^-$	$E2$	$687\binom{103}{79}$
5959.3	$14_1^+ \rightarrow 12_1^+$	$E2$	151(3)			$\rightarrow 5_2^-$	$E2$	$175\binom{35}{25}$
	$\rightarrow 12_3^+$	$E2$	114(7)			$\rightarrow 6_1^+$	$E1$	$1.8\binom{11}{4} \times 10^{-5}$
5272.4	$12_2^+ \rightarrow 10_1^+$	$E2$	$234 < B(E2) < 740$[f]		2646.4	$5^- \rightarrow 4^+$	$E1$	$3.26(6) \times 10^{-5}$
	$\rightarrow 10_2^+$	$E2$	< 850[f]					
5052.5	$12_1^+ \rightarrow 10_1^+$	$E2$	60(6)					
	$\rightarrow 10_2^+$	$E2$	12(1)					
	$\rightarrow 10_3^+$	$E2$	< 206[f]					
4195.2	$10_1^+ \rightarrow 8_1^+$	$E2$	$140\binom{5}{3}$					
	$\rightarrow 8_2^+$	$E2$	< 15.4[f]					
3484.7	$8_2^+ \rightarrow 8_1^+$	$M1$	> 0.4	$< 2.81 \times 10^4$				
3213.0	$8_1^+ \rightarrow 6_1^+$	$E2$	369(6)					
2626.9	$6_1^+ \rightarrow 4_1^+$	$E2$	81(4)					
1654.9	$4_1^+ \rightarrow 2_1^+$	$E2$	$926\binom{121}{96}$					
740.6	$2_1^+ \rightarrow 0_1^+$	$E2$	355(9)					

[a] $B(EL)\downarrow$ in $e^2\,\mathrm{fm}^{2L}$ ($E2$, 23.25 $e^2\mathrm{fm}^4 = 1$ W.u.; $E1$, $1.28 e^2\,\mathrm{fm}^2 = 1$ W.u.); $B(ML)\downarrow$ in $\mu_N^2\,\mathrm{fm}^{2L-2}$ ($M1$, 1.79 $\mu_N^2 = 1$ W.u.).
[b] All multipole strengths for mixed $E2/M1$ transitions calculated with the smaller δ solutions from Table II.
[c] Calculated for $\delta = 0$.
[d] No $B(E2)$ limits could be calculated for the 985-keV $\left(16_1^+ \rightarrow 14_1^+\right)$ transition due to unknown γ ray intensity.
[e] Calculated for $\delta < 0.7$ (see Table II).
[f] Only limits calculated for $B(\sigma L)$ values due to uncertainty in the level total deexcitation intensity.

energy. We note the absence of hindered transitions on both parity sides in ^{88}Mo, in contrast to ^{90}Mo.

The fewer particles in the $\nu(g_{9/2})$ shell for ^{90}Mo causes accidental unfavorable spin and seniority couplings. Thus, the 16_1^+ state obviously is not a pure $v = 4$ state of a fully aligned $[\pi(g_{9/2})_8^2 \nu(g_{9/2})_8^{-2}]$ configuration which would decay via a fast $16^+ \rightarrow 15^+ \rightarrow 14^+$ $M1$ cascade. However, the $M1$ transition from the 16_1^+ state is 437 times hindered (see Table VI), while the $B(E2)$ value is strongly enhanced. The $B(M1)$ strength of the $17_1^+ \rightarrow 16_1^+$ transition is also remarkably reduced which is evidence for a strong seniority mixing of the yrast 16^+ state being most probably what we call a seniority isomer. Another such candidate is the 20_3^+ state whose structure causes the $21_1^+ \rightarrow 20_3^+$ $M1$ transition to be 35 times hindered. It should be mentioned that the $B(E2)$ strengths of the yrast 12^+ state imply that, although being long lived, this state is certainly not a seniority isomer and its long lifetime can be understood merely by taking into account the reduced energies of the deexciting $E2$ transitions. The direct comparison of the $B(E2)$ strengths and branchings of the yrast 12^+ states in ^{88}Mo and ^{90}Mo (see Tables V and VI) shows that they have fairly similar structure, though the first two 10^+ states are most probably interchanged in the two nuclei. However, the structure of the 12_1^+ state and the two observed 10^+ states in ^{90}Mo provide a challenging test for the shell model calculations. This will be discussed in Sec. IV.

B. Negative parity states

Negative parity states in ^{88,90}Mo can be constructed by at least two proton particles or neutron holes in the $2p_{1/2}$ and $1g_{9/2}$ shells which couple to spins 4 or 5. Indeed, the 5^- states are the lowest negative parity states in both nuclei observed in heavy ion reactions [5,7,16]. However, their decays cannot be directly investigated within the shell model because they deexcite via $E1$ transitions which are forbidden even in the $1g_{9/2}, 2p_{1/2}, 2p_{3/2}, 1f_{5/2}$ configuration space. According to the transition probabilities, the differences in the structure of the negative parity states in ^{88}Mo and ^{90}Mo seem to be more profound than for their positive parity states. This is

TABLE VI. Comparison between experimantal reduced transition probabilities in ^{90}Mo and shell model predictions using two different residual interactions. σL denotes the lowest multipole which is visible via γ radiation. For mixed transitions, $\tilde{\sigma}L + 1$ denotes the next higher multipole.

E_x	$I_i^\pi \rightarrow I_f^\pi$		σL	Positive parity states [a]					
				Experiment		GF-2		SD-1	
[keV]	[$\hbar$]	[$\hbar$]		$B(\sigma L)\downarrow$	$B(\tilde{\sigma}L+1)\downarrow$	$B(\sigma L)\downarrow$	$B(\tilde{\sigma}L+1)\downarrow$	$B(\sigma L)\downarrow$	$B(\tilde{\sigma}L+1)\downarrow$
12016.6	23_1^+	$\rightarrow 21_1^+$	$E2$	> 30		n.a.[b]		n.a.	
		$\rightarrow 22_1^+$	$M1$	$> 4.0 \times 10^{-2}$ [c]		n.a.		n.a.	
		$\rightarrow 22_2^+$	$M1$	$> 9.7 \times 10^{-3}$ [c]		n.a.		n.a.	
11135.9	22_1^+	$\rightarrow 21_1^+$	$M1$	> 26	$> 6.6 \times 10^4$	n.a.	n.a.	n.a.	n.a.
10855.7	21_1^+	$\rightarrow 20_2^+$	$M1$	$0.17\binom{6}{3}$	$164\binom{68}{33}$	n.a.	n.a.	n.a.	n.a.
		$\rightarrow 20_3^+$	$M1$	$5(2) \times 10^{-2}$		n.a.		n.a.	
10235.2	20_2^+	$\rightarrow 18_1^+$	$E2$	$96\binom{44}{23}$		n.a.		n.a.	
		$\rightarrow 19_2^+$	$M1$	$0.7\binom{4}{2}$	$< 5.2 \times 10^3$	n.a.	n.a.	n.a.	n.a.
8525.4	18_1^+	$\rightarrow 16_1^+$	$E2$	$31\binom{9}{6}$		64		53	
		$\rightarrow 17_1^+$	$M1$	$2.2\binom{6}{4}$ [c]		2.4	93	3.0	93
8066.8	17_1^+	$\rightarrow 15_1^+$	$E2$	$24\binom{5}{4}$		39		33	
		$\rightarrow 15_2^+$	$E2$	$100\binom{23}{16}$		135		57	
		$\rightarrow 16_1^+$	$M1$	$4.0\binom{10}{6} \times 10^{-3}$ [c]		1.0×10^{-2}	0.20	6.0×10^{-3}	1.6×10^{-2}
		$\rightarrow 16_2^+$	$M1$	$5.8\binom{16}{7} \times 10^{-2}$ [c]		0.39	32	5.8×10^{-2}	0.29
6746.2	16_1^+	$\rightarrow 15_1^+$	$M1$	$4.1\binom{10}{7} \times 10^{-3}$	$1.9\binom{5}{3} \times 10^3$	2.4	108	2.2	86
6148.2	15_1^+	$\rightarrow 14_1^+$	$M1$	> 0.6	> 270	1.3×10^{-3}	0.76	2.8×10^{-2}	0.53
		$\rightarrow 14_2^+$	$M1$	> 2.6	$> 6.6 \times 10^3$	4.1	193	4.2	163
5903.7	14_2^+	$\rightarrow 13_1^+$	$M1$	$0.16\binom{6}{3}$	$140\binom{120}{50}$	5.1	224	3.8	174
5625.0	14_1^+	$\rightarrow 12_1^+$	$E2$	$77\binom{17}{12}$		94		60	
		$\rightarrow 13_1^+$	$M1$	$0.45(6)$[c]		2.7×10^{-2}	0.39	2.2×10^{-3}	9.0×10^{-3}
5377.2	13_1^+	$\rightarrow 12_1^+$	$M1$	$7\binom{4}{2} \times 10^{-2}$	$13\binom{14}{9}$	2.8	118	3.3	111
4555.8	12_1^+	$\rightarrow 10_1^+$	$E2$	$28\binom{6}{4}$		5.1×10^{-2}		0.41	
		$\rightarrow 10_2^+$	$E2$	$60\binom{13}{9}$		122		102	
4192.5	10_2^+	$\rightarrow 8_1^+$	$E2$	> 33		105		84.9	
		$\rightarrow 8_2^+$	$E2$	> 1.2		71		1.2	
		$\rightarrow 10_1^+$	$M1$	> 0.12[c]		4.3	328	2.3	162
4079.0	10_1^+	$\rightarrow 8_2^+$	$E2$	$45\binom{12}{8}$		98		61	
3106.3	8_2^+	$\rightarrow 8_1^+$	$M1$	$0.7\binom{4}{2}$		0.55	21	9.1	222

TABLE VI. *(Continued).*

E_x [keV]	$I_i^\pi \to I_f^\pi$ [$\hbar$]	σL	Negative parity states[a] Experiment $B(\sigma L)\downarrow$	Experiment $B(\tilde{\sigma}L+1)\downarrow$	GF-2 $B(\sigma L)\downarrow$	GF-2 $B(\tilde{\sigma}L+1)\downarrow$	SD-1 $B(\sigma L)\downarrow$	SD-1 $B(\tilde{\sigma}L+1)\downarrow$
7515.1	$17_1^- \to 15_1^-$	$E2$	$105\binom{42}{23}$		128		19	
	$\to 16_1^-$	$M1$	$0.21\binom{10}{5}$	$< 4.8 \times 10^3$	1.8	79	8.0×10^{-2}	4.5
	$\to 16_1^+$	$E1$	$2.7\binom{6}{4} \times 10^{-5}$		n.a.[b]		n.a.	
7385.6	$16_1^- \to 15_1^-$	$M1$	$1.4\binom{15}{5} \times 10^{-3}$	$344\binom{108}{66}$	0.14	9.0	0.64	21
6643.1	$15_1^- \to 13_1^-$	$E2$	$325\binom{40}{31}$		206		144	
	$\to 13_2^-$	$E2$	$59\binom{32}{15}$		45		4.3	
	$\to 14_1^-$	$M1$	1.2(2)[c]		0.75	50	6.8×10^{-2}	0.97
	$\to 14_1^+$	$E1$	$7(1) \times 10^{-5}$		n.a.		n.a.	
6475.8	$14_1^- \to 13_1^-$	$M1$	$< 2.2 \times 10^{-2}$	$1.0\binom{19}{4} \times 10^3$	1.4	84	4.4	132
	$\to 13_2^-$	$M1$	$4\binom{8}{2} \times 10^{-3}$ [c]		0.13	6.9×10^{-2}	1.0×10^{-4}	2.8×10^{-4}
	$\to 13_3^-$	$M1$	$5\binom{10}{2} \times 10^{-2}$ [c]		1.5	67	1.0×10^{-3}	2.0×10^{-3}
5699.6	$13_1^- \to 11_1^-$	$E2$	$610\binom{440}{180}$		238		12	
	$\to 12_1^+$	$E1$	$7\binom{10}{2} \times 10^{-5}$		n.a.		n.a.	
4842.0	$11_1^- \to 9_1^-$	$E2$	$197\binom{37}{27}$		264		93	
	$\to 10_2^+$	$E1$	$1.5\binom{9}{5} \times 10^{-5}$		n.a.		n.a.	
4297.7	$9_1^- \to 7_1^-$	$E2$	$84\binom{22}{15}$		415		155	
	$\to 7_2^-$	$E2$	$17\binom{5}{3}$		0.38		20	
3367.4	$7_1^- \to 5_1^-$	$E2$	$> 1.5 \times 10^3$		338		161	
	$\to 5_2^-$	$E2$	$> 2.2 \times 10^3$		7.0		64	
	$\to 6_1^+$	$E1$	$> 6.7 \times 10^{-4}$		n.a.		n.a.	
2548.8	$5_1^- \to 4_1^+$	$E1$	$1.7\binom{3}{2} \times 10^{-4}$		n.a.		n.a.	

[a] $B(EL)\downarrow$ in $e^2\,\mathrm{fm}^{2L}$ ($E2$, 23.96 $e^2\,\mathrm{fm}^4 = 1$ W.u.; $E1$, 1.29 $e^2\,\mathrm{fm}^2 = 1$ W.u.); $B(ML)\downarrow$ in $\mu_N^2\,\mathrm{fm}^{2L-2}$ ($M1$, 1.79$\mu_N^2 = 1$ W.u.).
[b] Not allowed in configuration space.
[c] Calculated for $\delta = 0$.

quite understandable in the most restricted model space, since the only possible neutron partition in ^{90}Mo is $\left[\nu(p_{1/2})^{-1}\nu(g_{9/2})^{-1}\right]_J$ ($J = 4, 5$). In ^{88}Mo, the larger number of $g_{9/2}$ neutron holes causes a complex interplay between proton and neutron excitations which, for instance, lifts the excitation energies of the states with even spins, none of them being observed experimentally [5]. As will be discussed in Sec. IV, such states in ^{90}Mo deexcite via strongly mixed dipole-quadrupole transitions which are caused by an internal structure resembling the unfavored signature in rotational bands. We point to the strongly hindered $M1$ transitions from the 7386-keV ($16_1^- \to 15_1^-$) and the 6476-keV ($14_1^- \to 13_{1,2}^-$) levels in ^{90}Mo whose $M1$ hindrance factors vary in the range 6×10^3–1.7×10^4. As can be seen from their mixing ratios (see Table I), these transitions have predominant quadrupole character. On the other hand, their feeders have rather moderate $B(M1)$ strengths. Another noticeable difference is presented by the $B(E2)$ strengths of some states in the low and intermediate spin regions of the two nuclei. In ^{90}Mo, the $7_1^- \to 5_1^-$ transition with $B(E2) > 62$ W.u. and the $7_1^- \to 5_2^-$ transition with $B(E2) > 91$ W.u. are strongly enhanced. We observe the same effect in the 11_1^- and 13_1^- states in ^{88}Mo which deexcite by transitions with strengths of 43 W.u. ($11_1^- \to 9_1^-$) and 77 W.u. ($13_1^- \to 11_1^-$). This means that the $5_{1,2}^-$ and 7_1^- states in ^{90}Mo are either strongly mixed by overlapping partitions of different seniorities or contain core components, as opposed to ^{88}Mo whose low lying negative parity states should have more pure character. The reasons for the enhancement of $E2$ transitions in ^{88}Mo are probably of the same nature.

IV. SHELL MODEL CALCULATIONS IN ^{90}Mo AND INTERPRETATION

It is well known that excited states in $N = 48, 49$, and 50 isotone series above $Z = 38$ can be well described by the shell model using a ^{88}Sr core with valence protons and neutron holes in the $1g_{9/2}$ and $2p_{1/2}$ orbits [15,42–44]. This is mainly due to the $N = 50$ shell gap which is considerably larger than those at $Z = 38$ and $Z = 40$. In recent work on ^{90}Mo [7], shell model calculations have been performed within an extended model space consisting of four proton orbits below $Z = 50$ and six neutron orbits which included $2d_{5/2}$, $2d_{3/2}$, and $3s_{1/2}$. It has been shown for both parities that up to spin $19\hbar$, no significant contributions to the wave functions from proton and neutron partitions outside the $2p_{1/2}$ and $1g_{9/2}$ orbits arise. The fact that seniority is an excellent quantum number for $N = 50$ nuclei (see [42] and references therein) and is almost conserved in $g_{9/2}^n$ proton configuration [15] gave rise to simple seniority classification schemes in several neutron deficient Nb, Mo, and Tc isotopes [1,5,6,9,10].

We compare the experimental information for ^{90}Mo

with two different shell model calculations in order to see how sensitively the wave functions of states in the intermediate spin range depend on the residual interaction and how well the seniority classification works. Both calculations use a ^{88}Sr core with active protons and neutrons in the $1g_{9/2}$ and $2p_{1/2}$ orbits but differ from each other by the residual interactions used. The first set, denoted by GF-2, utilizes the two-body matrix elements (TBME) and the four single-particle energies deduced by Gross and Frenkel [15]. The $T = 1$ neutron-neutron TBME are obtained from the proton-proton TBME by subtracting out the Coulomb energy shifts since this interaction has been designed to preserve charge independence. The other calculation, denoted by SD-1, was performed with TBME deduced from a surface δ interaction (SDI) [45] with interaction strength of $A_0 = A_1 = 0.48$. In both calculations, the experimental transition energies have been used to calculate the transition probabilities. More details concerning the two calculations and a list of the input parameters can be found in [10].

Figure 6 presents a comparison of experimental and theoretical excitation energies in ^{90}Mo. On the left-hand side, the positive parity states are shown. The right-hand side illustrates negative parity states. In order to optimize the overall agreement between theory and experiment, the theoretical levels were shifted. The definitions for this binding energy shift (BES) and the mean level deviation (MLD) can be found in [15]. For the GF-2 calcualtion, the fit to 35 states in ^{90}Mo between the 2549-keV 5^- and the 9444-keV 19^+ levels resulted in BES = 281 keV and MLD = 117 keV. The SD-1 interaction gives a smaller BES of 192 keV but a larger MLD of 170 keV.

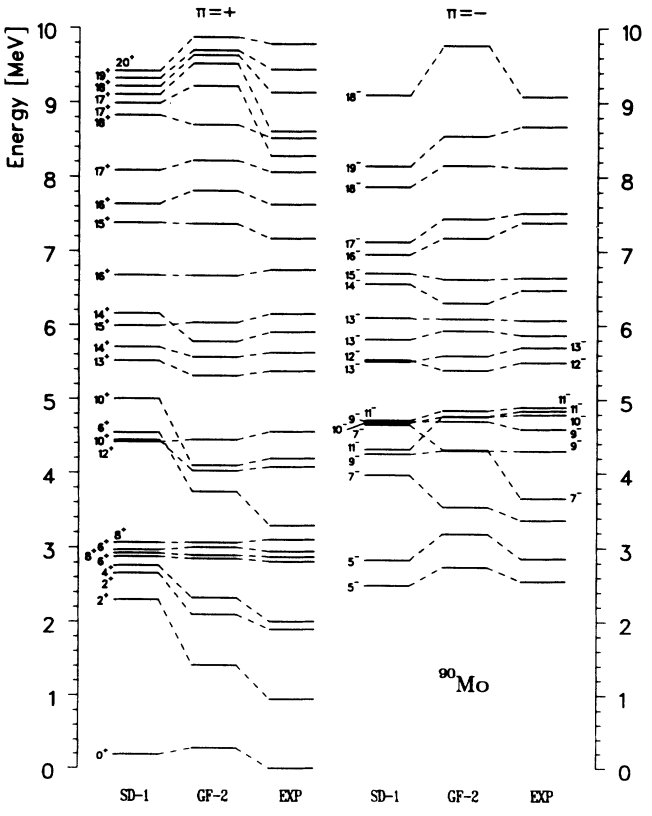

FIG. 6. Comparison of experimental level energies in ^{90}Mo and RITSSCHIL shell model calculations within the $p_{1/2}$, $g_{9/2}$ configuration space with fitted two-body matrix elements (GF-2) [15] and calculated two-body matrix elements with a surface δ interaction (SD-1) [45]. See text for details.

Tables VII and VIII list the calculated main partitions of several states in ^{90}Mo. A comparison between calculated and experimental branchings is presented in Table IX. Previous investigations of ^{90}Mo [17,44] have found almost pure aligned $\nu(g_{9/2})_8^{-2}$ and $\pi(g_{9/2})_8^2$ configurations for the 8_1^+ and 8_2^+ states, respectively, although they cannot be interpreted completely in this way. As can be seen from Table VII, GF-2 predicts that the aligned neutron and proton $v = 2$ partitions amount to some 70% of the wave functions. Nevertheless, an almost pure $8_2^+ \rightarrow 8_1^+$ $M1$ transition is favored (see Table I), probably due to weak $v = 4$ contributions. The branching ratio and the $B(M1; 8_2^+ \rightarrow 8_1^+)$ strength are nicely reproduced by the effective residual interaction. SD-1 predicts strong mixing of the two $v = 2$ partitions in both 8^+ states, overestimating the $B(M1)$ value (see Table VI). The SDI enhances the aligned proton-proton and neutron-neutron contributions as can be observed in the wave functions of the 15_2^+, 16_2^+, 17_1^+, and 18_1^+ states, and in the 5_2^-, 7_1^-, 9_2^-, 11_1^-, 13_3^-, and 14_1^- states.

The structures of the first two 10^+ states and the yrast 12^+ state seem to be crucial for testing the reliability of the calculations in the intermediate spin region. It has been suggested [17,44] that the observed separate $12_1^+ \rightarrow 10_1^+ \rightarrow 8_2^+$ and $12_1^+ \rightarrow 10_2^+ \rightarrow 8_1^+$ cascades imply a highly mixed structure of the yrast 12^+ state, but almost pure $[\pi(g_{9/2})_8^2 \nu(g_{9/2})_2^{-2}]$ and $[\pi(g_{9/2})_2^2 \nu(g_{9/2})_8^{-2}]$ configurations for the 10_1^+ and the 10_2^+ states, respectively. However, both calculations predict mixed wave functions for the two 10^+ states. This leads to a poor reproduction of the branching ratios from the 12^+ state and, for SD-1, to strong energy shifts of the two 10^+ levels due to the overestimated pairing correlations. As indicated by the main partitions listed in Table VII, the $E2$ transitions in the two cascades are generated by several 4–8% partitions in the two 10^+ states. However, these transitions are not hindered, which results in very unstable calculations. The long lifetime of the level and hence the sum of the partial transition probabilities are almost perfectly reproduced by the two calculations. Therefore, we closely investigated this problem by linearly mixing the wave functions of the two 10^+ states, preserving their normalization and orthogonality in such a manner that the branching ratios from the yrast 12^+ state get reproduced. This can be done by varying the single mixing parameter α in the following linear system:

$$\left|\widetilde{10_1^+}\right\rangle = \alpha \left|10_2^+\right\rangle + \sqrt{1-\alpha^2}\left|10_1^+\right\rangle ,$$

$$\left|\widetilde{10_2^+}\right\rangle = \sqrt{1-\alpha^2}\left|10_2^+\right\rangle - \alpha \left|10_1^+\right\rangle ,$$

where $\left|10_1^+\right\rangle$ and $\left|10_2^+\right\rangle$ are the initial wave functions. Using the calculated multipole GF-2 matrix elements, it was found that 34.3% mixing between the two states is

required to achieve perfect agreement with the experimental branching ratios. More interesting is that the new 10_1^+ state consists of 70% of the $[\pi(g_{9/2})_8^2\nu(g_{9/2})_2^{-2}]$ partition and only 0.2% of the $[\pi(g_{9/2})_2^2\nu(g_{9/2})_8^{-2}]$ configuration in contrast to the modified 10_2^+ state where this ratio is 0.3:69.7. This structure perfectly explains the observed almost pure decays of the 10_1^+ and the 10_2^+ states into the 8_2^+ and 8_1^+ levels, respectively. Furthermore, the calculated $E2$ strengths, $B(E2, 12^+ \to \widetilde{10_1^+}) = 44e^2$ fm^4 and $B(E2, 12^+ \to \widetilde{10_2^+}) = 78e^2$ fm^4 are in far better agreement with the experimental values than the original predictions of GF-2. These results lead to the conclusion that the interpretation of the 10^+ states as almost pure configurations of the above type is the most reasonable one in this model space. Both calculated and experimental $B(E2)$ strengths imply that the long lifetime of the

TABLE VII. Main partitions of wave functions of positive parity states in ^{90}Mo. The wave functions are given in terms of subshell occupations by unpaired protons π or neutrons ν which couple to certain spin. v denotes the partition seniority.

Positive parity states						
E_x [keV]	I^π [$\hbar$]	Wave function		v	GF-2 [%]	SD-1 [%]
2847.8	8_1^+		$\nu(g_{9/2})_8^{-2}$	2	71.9	53.0
		$\pi(g_{9/2})_2^2$	$\nu(g_{9/2})_8^{-2}$	4	15.4	3.2
		$\pi(g_{9/2})_2^2$	$\nu(g_{9/2})_6^{-2}$	4	6.1	0.7
		$\pi(g_{9/2})_8^2$		2	1.7	29.4
3106.3	8_2^+	$\pi(g_{9/2})_8^2$		2	74.1	58.7
		$\pi(g_{9/2})_8^2$	$\nu(g_{9/2})_2^{-2}$	4	12.6	1.6
		$\pi(g_{9/2})_6^2$	$\nu(g_{9/2})_2^{-2}$	4	6.7	0.4
			$\nu(g_{9/2})_8^{-2}$	2	1.4	32.0
4079.0	10_1^+	$\pi(g_{9/2})_8^2$	$\nu(g_{9/2})_2^{-2}$	4	43.0	16.1
		$\pi(g_{9/2})_2^2$	$\nu(g_{9/2})_8^{-2}$	4	28.4	18.9
		$\pi(g_{9/2})_8^2$	$\nu(g_{9/2})_4^{-2}$	4	6.2	8.4
		$\pi(g_{9/2})_4^2$	$\nu(g_{9/2})_8^{-2}$	4	4.5	7.1
		$\pi(g_{9/2})_6^2$	$\nu(g_{9/2})_4^{-2}$	4	4.0	3.6
4192.5	10_2^+	$\pi(g_{9/2})_2^2$	$\nu(g_{9/2})_8^{-2}$	4	41.5	20.2
		$\pi(g_{9/2})_8^2$	$\nu(g_{9/2})_2^{-2}$	4	27.5	26.6
		$\pi(g_{9/2})_4^2$	$\nu(g_{9/2})_6^{-2}$	4	8.6	9.2
		$\pi(g_{9/2})_6^2$	$\nu(g_{9/2})_4^{-2}$	4	6.8	10.6
		$\pi(g_{9/2})_4^2$	$\nu(g_{9/2})_8^{-2}$	4	6.4	6.4
4555.8	12^+	$\pi(g_{9/2})_8^2$	$\nu(g_{9/2})_8^{-2}$	4	19.3	24.9
		$\pi(g_{9/2})_6^2$	$\nu(g_{9/2})_6^{-2}$	4	17.2	13.8
		$\pi(g_{9/2})_4^2$	$\nu(g_{9/2})_8^{-2}$	4	17.2	9.6
		$\pi(g_{9/2})_8^2$	$\nu(g_{9/2})_4^{-2}$	4	17.0	9.3
5377.2	13^+	$\pi(g_{9/2})_8^2$	$\nu(g_{9/2})_8^{-2}$	4	64.7	45.0
		$\pi(g_{9/2})_6^2$	$\nu(g_{9/2})_8^{-2}$	4	16.5	21.9
		$\pi(g_{9/2})_8^2$	$\nu(g_{9/2})_6^{-2}$	4	14.0	20.1
5625.0	14_1^+	$\pi(g_{9/2})_6^2$	$\nu(g_{9/2})_8^{-2}$	4	51.9	44.8
		$\pi(g_{9/2})_8^2$	$\nu(g_{9/2})_6^{-2}$	4	43.9	45.5
5903.7	14_2^+	$\pi(g_{9/2})_8^2$	$\nu(g_{9/2})_8^{-2}$	4	81.8	88.5
6148.2	15_1^+	$\pi(g_{9/2})_8^2$	$\nu(g_{9/2})_8^{-2}$	4	95.1	91.1
7170.9	15_2^+	$\pi(g_{9/2})_8^2$	$\nu(g_{9/2})_8^{-2}$	4	67.9	32.7
		$\pi(g_{9/2})_7^4$	$\nu(g_{9/2})_8^{-2}$	6	16.1	6.0
		$[\pi(p_{1/2})^1\pi(g_{9/2})^3]_{11}$	$[\nu(p_{1/2})^1\nu(g_{9/2})^{-1}]_5$	6	1.4	43.2
6746.2	16_1^+	$\pi(g_{9/2})_8^2$	$\nu(g_{9/2})_8^{-2}$	4	97.7	96.8
7629.6	16_2^+	$\pi(g_{9/2})_8^2$	$\nu(g_{9/2})_8^{-2}$	4	63.4	3.7
		$\pi(g_{9/2})_{10}^4$	$\nu(g_{9/2})_6^{-2}$	6	22.6	0.3
		$[\pi(p_{1/2})^1\pi(g_{9/2})^3]_{11}$	$[\nu(p_{1/2})^1\nu(g_{9/2})^{-1}]_5$	6	0.3	88.8
8066.8	17^+	$\pi(g_{9/2})_{10}^4$	$\nu(g_{9/2})_8^{-2}$	6	59.9	43.6
		$\pi(g_{9/2})_9^4$	$\nu(g_{9/2})_8^{-2}$	6	22.4	19.3
		$\pi(g_{9/2})_{12}^4$	$\nu(g_{9/2})_6^{-2}$	6	9.0	17.7
		$\pi(g_{9/2})_{12}^4$	$\nu(g_{9/2})_8^{-2}$	6	8.7	19.3
8525.4	18^+	$\pi(g_{9/2})_{10}^4$	$\nu(g_{9/2})_8^{-2}$	6	83.3	66.6
		$\pi(g_{9/2})_{12}^4$	$\nu(g_{9/2})_6^{-2}$	6	9.5	11.2
		$\pi(g_{9/2})_{12}^4$	$\nu(g_{9/2})_8^{-2}$	6	7.2	22.1
9443.9	19^+	$\pi(g_{9/2})_{12}^4$	$\nu(g_{9/2})_8^{-2}$	6	100.0	100.0
9788.0	20^+	$\pi(g_{9/2})_{12}^4$	$\nu(g_{9/2})_8^{-2}$	6	100.0	100.0

yrast 12^+ level is mainly caused by the reduced energies of the deexciting transitions, so that this state can hardly be interpreted as a seniority isomer (see also Sec. III).

A similar analysis was carried out with the 15_1^+ state and the first two 14^+ states which exhibit a similar branching ratio problem (see Table IX). Both GF-2 and SD-1 predict a fully aligned $[\pi(g_{9/2})_8^2\nu(g_{9/2})_8^{-2}]$ configuration for the 14_2^+ state and a mixed structure of

TABLE VIII. Main partitions of wave functions of negative parity states in ^{90}Mo. The wave functions are given in terms of subshell occupations by unpaired protons π or neutrons ν which couple to certain spin. v denotes the partition seniority.

Negative parity states						
E_x [keV]	I^π [$\hbar$]	Wave function		v	GF-2 [%]	SD-1 [%]
2548.8	5_1^-	$[\pi(p_{1//2})^1\pi(g_{9/2})^1]_5$		2	75.8	52.4
			$[\nu(p_{1/2})^1\nu(g_{9/2})^{-1}]_5$	2	2.2	41.9
2859.2	5_2^-		$[\nu(p_{1/2})^1\nu(g_{9/2})^{-1}]_5$	2	74.2	42.8
		$\pi(g_{9/2})_2^2$	$[\nu(p_{1/2})^1\nu(g_{9/2})^{-1}]_5$	4	12.3	2.1
		$[\pi(p_{1/2})^1\pi(g_{9/2})^1]_5$		2	1.1	39.2
3367.4	7_1^-	$[\pi(p_{1/2})^1\pi(g_{9/2})^3]_7$		4	44.2	75.7
		$[\pi(p_{1/2})^1\pi(g_{9/2})^1]_5$	$\nu(g_{9/2})_2^{-2}$	4	39.1	8.0
3659.7	7_2^-	$[\pi(p_{1/2})^1\pi(g_{9/2})^1]_5$	$\nu(g_{9/2})_2^{-2}$	4	29.9	39.4
		$[\pi(p_{1/2})^1\pi(g_{9/2})^3]_7$		4	29.4	8.6
		$[\pi(p_{1/2})^1\pi(g_{9/2})^3]_6$	$\nu(g_{9/2})_2^{-2}$	6	11.4	3.3
4297.7	9_1^-	$[\pi(p_{1/2})^1\pi(g_{9/2})^3]_7$	$\nu(g_{9/2})_2^{-2}$	6	33.4	1.1
		$[\pi(p_{1/2})^1\pi(g_{9/2})^3]_9$		4	28.0	76.1
		$[\pi(p_{1/2})^1\pi(g_{9/2})^1]_5$	$\nu(g_{9/2})_4^{-2}$	4	19.0	0.9
4594.2	9_2^-	$[\pi(p_{1/2})^1\pi(g_{9/2})^3]_9$		4	34.3	5.2
		$[\pi(p_{1/2})^1\pi(g_{9/2})^1]_5$	$\nu(g_{9/2})_4^{-2}$	4	26.3	24.0
4842.0	11^-	$[\pi(p_{1/2})^1\pi(g_{9/2})^3]_{11}$		4	27.9	72.3
		$[\pi(p_{1/2})^1\pi(g_{9/2})^1]_5$	$\nu(g_{9/2})_8^{-2}$	4	14.8	0.2
		$[\pi(p_{1/2})^1\pi(g_{9/2})^3]_9$	$\nu(g_{9/2})_2^{-2}$	6	11.7	0.8
		$\pi(g_{9/2})_8^2$	$[\nu(p_{1/2})^1\nu(g_{9/2})^{-1}]_5$	4	3.1	16.2
5699.6	13_1^-	$[\pi(p_{1/2})^1\pi(g_{9/2})^3]_9$	$\nu(g_{9/2})_4^{-2}$	6	17.1	11.4
		$[\pi(p_{1/2})^1\pi(g_{9/2})^3]_{11}$	$\nu(g_{9/2})_2^{-2}$	6	16.9	6.8
		$[\pi(p_{1/2})^1\pi(g_{9/2})^3]_7$	$\nu(g_{9/2})_6^{-2}$	6	15.8	5.7
		$[\pi(p_{1/2})^1\pi(g_{9/2})^3]_6$	$\nu(g_{9/2})_8^{-2}$	6	13.3	7.7
5863.7	13_2^-	$[\pi(p_{1/2})^1\pi(g_{9/2})^1]_5$	$\nu(g_{9/2})_8^{-2}$	4	65.2	75.3
		$[\pi(p_{1/2})^1\pi(g_{9/2})^3]_{11}$	$\nu(g_{9/2})_2^{-2}$	6	10.7	0
6064.8	13_3^-	$[\pi(p_{1/2})^1\pi(g_{9/2})^3]_{11}$	$\nu(g_{9/2})_2^{-2}$	6	34.4	0.4
		$[\pi(p_{1/2})^1\pi(g_{9/2})^3]_7$	$\nu(g_{9/2})_8^{-2}$	6	24.2	0.2
		$[\pi(p_{1/2})^1\pi(g_{9/2})^3]_6$	$\nu(g_{9/2})_8^{-2}$	6	10.9	0.4
		$[\pi(p_{1/2})^1\pi(g_{9/2})^1]_5$	$\nu(g_{9/2})_8^{-2}$	4	10.7	17.3
		$\pi(g_{9/2})_8^2$	$[\nu(p_{1/2})^1\nu(g_{9/2})^{-1}]_5$	4	0.9	73.8
6475.8	14^-	$[\pi(p_{1/2})^1\pi(g_{9/2})^3]_7$	$\nu(g_{9/2})_8^{-2}$	6	50.0	13.2
		$[\pi(p_{1/2})^1\pi(g_{9/2})^3]_6$	$\nu(g_{9/2})_8^{-2}$	6	23.9	5.2
		$[\pi(p_{1/2})^1\pi(g_{9/2})^3]_9$	$\nu(g_{9/2})_8^{-2}$	6	10.2	17.8
		$[\pi(p_{1/2})^1\pi(g_{9/2})^3]_{11}$	$\nu(g_{9/2})_8^{-2}$	6	4.6	29.3
6643.1	15^-	$[\pi(p_{1/2})^1\pi(g_{9/2})^3]_7$	$\nu(g_{9/2})_8^{-2}$	6	34.6	2.4
		$[\pi(p_{1/2})^1\pi(g_{9/2})^3]_9$	$\nu(g_{9/2})_6^{-2}$	6	30.9	32.1
		$[\pi(p_{1/2})^1\pi(g_{9/2})^3]_{11}$	$\nu(g_{9/2})_4^{-2}$	6	22.1	35.2
7385.6	16^-	$[\pi(p_{1/2})^1\pi(g_{9/2})^3]_9$	$\nu(g_{9/2})_8^{-2}$	6	38.9	12.6
		$[\pi(p_{1/2})^1\pi(g_{9/2})^3]_8$	$\nu(g_{9/2})_8^{-2}$	6	30.9	32.3
		$[\pi(p_{1/2})^1\pi(g_{9/2})^3]_{11}$	$\nu(g_{9/2})_6^{-2}$	6	20.7	49.2
7515.1	17^-	$[\pi(p_{1/2})^1\pi(g_{9/2})^3]_9$	$\nu(g_{9/2})_8^{-2}$	6	44.1	28.8
		$[\pi(p_{1/2})^1\pi(g_{9/2})^3]_{11}$	$\nu(g_{9/2})_8^{-2}$	6	34.4	55.1
		$[\pi(p_{1/2})^1\pi(g_{9/2})^3]_{11}$	$\nu(g_{9/2})_6^{-2}$	6	20.7	14.4
8123.6	18^-	$[\pi(p_{1/2})^1\pi(g_{9/2})^3]_{11}$	$\nu(g_{9/2})_8^{-2}$	6	99.9	99.9
8678.5	19^-	$[\pi(p_{1/2})^1\pi(g_{9/2})^3]_{11}$	$\nu(g_{9/2})_8^{-2}$	6	100.0	100.0

the yrast 14^+ state with the $[\pi(g_{9/2})^2_6\nu(g_{9/2})^{-2}_8]$ and $[\pi(g_{9/2})^2_8\nu(g_{9/2})^{-2}_6]$ partitions, each about 50% of the total wave function. In this case, only 17% mixing between the two initial GF-2 wave functions is required to satisfy the experimental branching ratios. In addition, similar to the results for the 12^+ state, the new $M1$ strengths $B(M1, 15^+ \rightarrow \widetilde{14^+_1}) = 0.65\mu^2_N$ and $B(M1, 15^+ \rightarrow \widetilde{14^+_2}) = 3.4\mu^2_N$ fit very well into the experimental data. Thus, fully aligned configurations seem to be energetically more favorable for ^{90}Mo than predicted by the GF calculations.

Another question is raised concerning the 13^+_1 state in light of the calculations. It has been observed [7,16] that the 14^+_1 state decays with 52% probability into the 12^+_1 state and with 48% into the 13^+ state. GF-2 and SD-1 predict branchings of 96:4 and 99:1 (see Table IX). The calculations correctly reproduce $B(E2; 14^+_1 \rightarrow 12^+_1)$ while the predicted $B(E2; 14^+_1 \rightarrow 13^+_1)$ value is smaller than the experimental one by an order of magnitude. Furthermore, $B(M1; 13^+_1 \rightarrow 12^+_1)$ is about 40 times overestimated in both calculations. The reason is the dominant $[\pi(g_{9/2})^2_8\nu(g_{9/2})^{-2}_8]$ partition which hinders dipole decay transitions from the two equally strong components $[\pi(g_{9/2})^2_6\nu(g_{9/2})^{-2}_8]$ and $[\pi(g_{9/2})^2_8\nu(g_{9/2})^{-2}_6]$ of the 14^+_1 state. The experimental $B(M1; 13^+_1 \rightarrow 12^+_1)$ strength of $0.07\mu^2_N$ and the nonvanishing multipole mixing ratio $\delta = 0.09(4)$ point to possible seniority $v = 6$ admixtures in the 13^+_1 state which the two calculations do not predict. We suggest much stronger $v = 6$ contributions to be responsible for the strong retardation and the large mixing ratio of the $16^+_1 \rightarrow 15^+_1$ transition. However, both calculations predict a pure $[\pi(g_{9/2})^2_8\nu(g_{9/2})^{-2}_8]$ configuration for the 15^+_1 and 16^+_1 states which would result in a fast dipole transition between them.

The structure of the 8067-keV 17^+_1 state is another illustration of the problems with the mixed structure of ^{90}Mo positive parity states. GF-2 and SD-1 predict similarly mixed configurations, but SD-1 slightly enhances the $[\pi(g_{9/2})^4_{12}\nu(g_{9/2})^{-2}_6]$ and $[\pi(g_{9/2})^4_{12}\nu(g_{9/2})^{-2}_8]$ components which leads to a very good reproduction of the branchings and the reduced transition strengths from this state.

On the negative parity side, the effective interaction

TABLE IX. Comparison between experimental and theoretical branching ratios in ^{90}Mo.

Positive parity states						Negative parity states [a]					
E_x	$I^\pi_i \rightarrow I^\pi_f$		b [%] [b]			E_x	$I^\pi_i \rightarrow I^\pi_f$		b [%] [b]		
[keV]	[$\hbar$]	[$\hbar$]	expt[c]	GF-2	SD-1	[keV]	[$\hbar$]	[$\hbar$]	expt[c]	GF-2	SD-1
2847.8	8^+_1	$\rightarrow 6^+_1$	100	100	100	3367.4	7^-_1	$\rightarrow 5^-_1$	≥ 88	100	96
3106.3	8^+_2	$\rightarrow 8^+_1$	100	100	100			$\rightarrow 5^-_2$	≤ 12	0	4
4079.0	10^+_1	$\rightarrow 8^+_1$	n.o.	73	37	4297.7	9^-	$\rightarrow 7^-_1$	96.9(3)	100	98
		$\rightarrow 8^+_2$	100	27	63			$\rightarrow 7^-_2$	3.1(3)	0	2
4192.5	10^+_2	$\rightarrow 8^+_1$	96.4(6)	68	87	4842.0	11^-_1	$\rightarrow 9^-$	100	97	100
		$\rightarrow 8^+_2$	1.3(3)	18	1			$\rightarrow 10^-$	n.o.	3	0
		$\rightarrow 10^+_1$	1.9(4)	14	12	5699.6	13^-_1	$\rightarrow 11^-_1$	100	94	36
4555.8	12^+	$\rightarrow 10^+_1$	65(3)	0	2			$\rightarrow 11^-_2$	n.o.	4	64
		$\rightarrow 10^+_2$	35(4)	100	98			$\rightarrow 12^-$	n.o.	2	0
5377.2	13^+	$\rightarrow 12^+$	100	100	100	6475.8	14^-	$\rightarrow 12^-$	n.o.	1	0
5625.0	14^+_1	$\rightarrow 12^+$	52(4)	96	99			$\rightarrow 13^-_1$	84(3)	82	100
		$\rightarrow 13^+$	48(4)	4	1			$\rightarrow 13^-_2$	3.7(5)	4	0
5903.7	14^+_2	$\rightarrow 13^+_1$	100	100	100			$\rightarrow 13^-_3$	12(3)	13	0
6148.2	15^+_1	$\rightarrow 14^+_1$	69(3)	0	6	6643.1	15^-_1	$\rightarrow 13^-_1$	70(3)	70	95
		$\rightarrow 14^+_2$	31(3)	100	94			$\rightarrow 13^-_2$	5(2)	6	1
6746.2	16^+_1	$\rightarrow 14^+_1$	n.o.	2	2			$\rightarrow 13^-_3$	n.o.	1	0
		$\rightarrow 15^+_1$	100	98	98			$\rightarrow 14^-$	25(3)	23	4
8066.8	17^+	$\rightarrow 15^+_1$	71(3)	54	88	7385.6	16^-	$\rightarrow 14^-$	n.o.	4	1
		$\rightarrow 15^+_2$ [d]	6(1)	4	3			$\rightarrow 15^-_1$	100	37	95
		$\rightarrow 16^+_1$	15(2)	18	2			$\rightarrow 15^-_2$	n.o.	59	4
		$\rightarrow 16^+_2$	8(1)	24	7	7515.1	17^-_1	$\rightarrow 15^-_1$	87(4)	54	67
8525.4	18^+_1	$\rightarrow 16^+_1$	16(2)	25	19			$\rightarrow 15^-_2$	n.o.	1	16
		$\rightarrow 16^+_2$	n.o.	2	0			$\rightarrow 16^-$	13(4)	45	17
		$\rightarrow 17^+$	84(2)	73	81	8123.6	18^-	$\rightarrow 17^-_1$	100	96	98
9443.9	19^+	$\rightarrow 17^+$	3(1)	8	3			$\rightarrow 17^-_2$	n.o.	4	2
		$\rightarrow 18^+_1$	79(2)	72	86	8678.5	19^-	$\rightarrow 17^-_1$	n.o.	3	2
		$\rightarrow 18^+_2$ [e]	18(2)	20	11			$\rightarrow 18^-$	100	97	98
9788.0	20^+	$\rightarrow 18^+$	32(3)	21	19						
		$\rightarrow 19^+$	68(3)	79	81						

[a] $E1$ transitions excluded from the branchings for better comparison.
[b] Theoretical branching ratios less than 1% are denoted with 0.
[c] Not observed branches denoted by n.o.
[d] Spin assignment proposed in this work.
[e] Transition observed in this work for the first time.

GF-2 reproduces the transition probabilities and branchings from states with odd spins above 7_1^- while the agreement for the yrast 7^- state itself is poor. Taking into account that the experimental level energies of the yrast and yrare 5^- and 7^- states are considerably lowered (see Fig. 6) compared to the predicted values, we suggest that these states may contain substantional core components and, thus, may lie outside our model space. The overall agreement for the SD-1 calculation is rather poor, though it assignes a predominant $\pi\left[(p_{1/2})^1(g_{9/2})^3\right]_9$ configuration to the 9_1^- state and reproduces its decay properties better than GF-2. The lower success of SDI for negative parity states can be explained with the favoring of the residual interaction between identical nucleons occupying the same orbit. However, the shell model calculations do not reproduce the observed large multipole mixing ratios of the $16_1^- \rightarrow 15_1^-$ and $14_1^- \rightarrow 13_1^-$ transitions. Both GF-2 and SD-1 predict mixed configurations for the 16_1^- and 14_1^- states which contain significant $\pi\left[(p_{1/2})^1(g_{9/2})^3\right]_J \nu(g_{9/2})_8^{-2}$ $(J = 6, 7, 8, 9)$ partitions. In fact, the experimental energies of the two states are lifted by more than one MLD from their GF-2 predicitions (see Fig. 6), implying that the most probable proton $\pi[(p_{1/2})^1_{1/2}(g_{9/2})^3_{13/2}]_7$, $\pi[(p_{1/2})^1_{1/2}(g_{9/2})^3_{17/2}]_9$ couplings are prefered due to isospin repulsion. In this case, only quadrupole transitions to the main partitions of the 15_1^- and 13_1^- states would be possible, in agreement with the experiment.

V. CONCLUSIONS

The present work completes the existing information for the neutron-deficient nuclei ^{88,90}Mo with a large number of mixing ratios and lifetimes. Among the well-known 8_1^+ isomeric state in ^{90}Mo, a second long-lived state was established at 12^+ with $\tau = 759(5)$ ps. The large amount of spectroscopic data has allowed us to make a detailed comparison between the excitation schemes of the two nuclei. In its ground state, ^{88}Mo appears to sustain a nearly spherical shape which probably performes quadrupole vibrations. The $E2$ transitions between $v = 4, 6$ positive parity states in ^{88}Mo have in general larger $B(E2)$ strengths than the corresponding transitions in ^{90}Mo which we trace back to the larger number of neutron holes in the $g_{9/2}$ neutron orbit. In ^{90}Mo, unfavorable spin and seniority coupling between valence nucleons leads to strongly hindered $M1$ transitions, referred to here as seniority isomers. Such candidates are the 16_1^+ and the 20_3^+ states. According to the Weisskopf units estimates, the 12_1^+ state is not hindered and can be fully understood in terms of partition mixing.

On the negative parity side, the equal number of proton particles and neutron holes in the $g_{9/2}$ shell in ^{88}Mo causes a complex interplay between the two types of excitations which leads to differences between the decay patterns of the two nuclei. $E2$ transitions between low lying negative parity states in ^{90}Mo are enhanced which implies either significant core excitations in their wave functions or strong seniority mixing.

The extensive experimental information on electromagnetic decay properties has allowed us to thoroughly test the predictions of the shell model for ^{90}Mo. Two different calculations for this nucleus are presented which can be summarized as follows:

(1) Most of the properties of positive parity states up to 18^+ and negative parity states up to 19^- can be understood in the smallest possible configuration space — $p_{1/2}$ and $g_{9/2}$ orbits — with the TBME of the residual interaction and the single-particle energies fixed by Gross and Frenkel [15]. The deduced mean level deviation of 117 keV is distinctly smaller than the average difference between yrast and yrare states of some 300 keV. The properties of yrare states are in general well reproduced in contrast to previous calculations in a more extended model space [7].

(2) The approach of deriving the TBME from the modified δ interaction is less successful especially for negative parity states where the interaction between valence nucleons in different orbits takes place.

(3) Both calculations favor the seniority of a state as a nearly good quantum number. There are, however, several strongly hindered $M1$ transitions which cannot be explained in this frame and others, whose decay properties could be well reproduced if a simple favored coupling scheme for the proton particles is suggested.

(4) The predictions concerning branching ratios and transition probabilities change dramatically if only minor changes in the components of some wave functions are proposed. The analysis of a recent g–factor measurement could possibly fix some of the ambiguities for low lying states [19].

ACKNOWLEDGMENTS

The help of Frank Moore for installing the code LILIFI is greatly acknowledged. We thank T.D. Johnson for carefully reading the manuscript and last but not least the crews and staff of the accelerators at Berlin and Cologne for their support. The γ spectra were analyzed with the code vs created by J. Theuerkauf, S. Esser, S. Krink, N. Nicolay, and H. Wolters, Universität zu Köln. This research was supported by Deutsches BMFT under Contract Nos. 06GÖ451 and KÖ06OK602I.

[1] A. Bödeker, K.P. Lieb, C.J. Gross, M.K. Kabadiyski, D. Rudolph, M. Weiszflog, J. Eberth, H. Grawe, J. Heese, and K.-H. Maier, Phys. Rev. C **48**, 1617 (1993).

[2] C.J. Gross, W. Gelletly, M.A. Bentley, H.G. Price, J. Simpson, K.P. Lieb, D. Rudolph, J.L. Durell, B.J. Varley, and S. Rastikerdar, Phys. Rev. C **44**, R2253 (1991).

[3] Ch. Winter, D.J. Blumenthal, P. Chowdhury, B. Crowell, P.J. Ennis, C.J. Lister, C.J. Gross, J. Heese, A. Jungclaus, K.P. Lieb, J. Eberth, and S. Skoda, Phys. Lett. B **258**, 289 (1991).

[4] Ch. Winter, D.J. Blumenthal, P. Chowdhury, B. Crowell, P.J. Ennis, S.J. Freeman, C.J. Lister, C.J. Gross, J.

Heese, A. Jungclaus, K.P. Lieb, D. Rudolph, M.A. Bentley, W. Gelletly, J.L. Durell, and B.J. Varley, Nucl. Phys. **A535**, 137 (1991).
[5] M. Weiszflog, K.P. Lieb, F. Cristancho, C.J. Gross, A. Jungclaus, D. Rudolph, H. Grawe, J. Heese, K.H. Maier, R. Schubart, J. Eberth, and S. Skoda, Z. Phys. A **342**, 257 (1992).
[6] M. Weiszflog, D. Rudolph, C.J. Gross, M.K. Kabadiyski, K.P. Lieb, H. Grawe, J. Heese, K.H. Maier, and J. Eberth, Z. Phys. A **344**, 395 (1993).
[7] M.K. Kabadiyski, F. Cristancho, C.J. Gross, A. Jungclaus, K.P. Lieb, D. Rudolph, H. Grawe, J. Heese, K.H. Maier, J. Eberth, S. Skoda, W.-T. Chou, and E.K. Warburton, Z. Phys. A **343**, 165 (1992).
[8] D. Rudolph, F. Cristancho, C.J. Gross, A. Jungclaus, K.P. Lieb, H. Grawe, J. Heese, K.H. Maier, J. Eberth, and S. Skoda, Z. Phys. A **342**, 121 (1992).
[9] D. Rudolph, C.J. Gross, M.K. Kabadiyski, K.P. Lieb, M. Weiszflog, H. Grawe, J. Heese, K.H. Maier, and J. Eberth, Phys. Rev. C **47**, 2574 (1993).
[10] D. Rudolph, C.J. Gross, A. Harder, M.K. Kabadiyski, K.P. Lieb, M. Weiszflog, J. Altmann, A. Dewald, J. Eberth, T. Mylaeus, H. Grawe, J. Heese, and K.-H. Maier, Phys. Rev. C **49**, 66 (1994).
[11] S.E. Arnell, D. Foltescu, H.A. Roth, Ö. Skeppstedt, A. Nilsson, S. Mitarai, and J. Nyberg, Phys. Scr. **47**, 142 (1993).
[12] J. Heese, H. Grawe, K.H. Maier, R. Schubart, F. Cristancho, C.J. Gross, A. Jungclaus, K.P. Lieb, D. Rudolph, J. Eberth, and S. Skoda, Phys. Rev. C (to be published).
[13] S.E. Arnell, D. Foltescu, H.A. Roth, Ö. Skeppstedt, A. Nilsson, S. Mitarai, and J. Nyberg, Phys. Scr. **47**, 355 (1993).
[14] S.E. Arnell, D. Foltescu, H.A. Roth, Ö. Skeppstedt, A. Nilsson, S. Mitarai, and J. Nyberg, Z. Phys. A **346**, 111 (1993).
[15] R. Gross and A. Frenkel, Nucl. Phys. **A267**, 85 (1976).
[16] S.E. Arnell, D. Foltescu, H.A. Roth, Ö. Skeppstedt, A. Nilsson, S. Mitarai, and J. Nyberg, Phys. Scr. **46**, 389 (1992).
[17] F.W.N. de Boer, C.A. Fields, L.E. Samuelson, and J. Sau, Nucl. Phys. **A388**, 303 (1982).
[18] Pr. Singh, R.G. Pillay, J.A. Sheikh, and H.G. Devare, Phys. Rev. C **45**, 2161 (1992).
[19] M. Weiszflog, J. Billowes, A. Harder, M.K. Kabadiyski, K.P. Lieb, A. Raguse, D. Rudolph, T. Burkhard, J. Eberth, T. Mylaeus, and S. Skoda (submitted to Phys. Lett. B).
[20] R.M. Lieder, H. Jaeger, A. Neskakis, and T. Venkova, Nucl. Instrum. Methods **220**, 363 (1984).
[21] M.K. Kabadiyski, K.P. Lieb, and D. Rudolph, Nucl. Phys. **A563**, 301 (1993).
[22] H.J. Rose and D.M. Brink, Rev. Mod. Phys. **39**, 306 (1967).
[23] T. Yamazaki, At. Data Nucl. Data Tables **3**, 1 (1967).
[24] J. Black and W. Gruhle, Nucl. Instrum. Methods **46**, 213 (1967).
[25] D.C. Camp and A.L. van Lehn, Nucl. Instrum. Methods **76**, 192 (1969).
[26] R.M. Steffen and K. Alder, in *Angular Distributions and Correlations of Gamma Rays – I. Theory*, edited by W.D. Hamilton (North-Holland, Amsterdam, 1975), Chap. XII.
[27] A.R. Poletti and E.K. Warburton, Phys. Rev. **137**, B595 (1965).
[28] F. Cristancho and K. P. Lieb, Nucl. Phys. **A524**, 518 (1991).
[29] J.P. Biersack and L.G. Haggmark, Nucl. Instrum. Methods **174**, 257 (1980).
[30] A. Gavron, Phys. Rev. C **21**, 230 (1980).
[31] H. Emling *et al.*, in "Proceedings of the Twenty-Second School on Physics, Zakopane, Poland," edited by R. Broda and Z. Stachura, Instytut Fizyki Jadrowej w Krakowie Report No. IFL 1956/PL, 1987 (unpublished), p. 151.
[32] A. Dewald, P. Sala, R. Wrzal, G. Böhm, D. Lieberz, G. Siems, R. Wirowski, K.O. Zell, A. Gelberg, P. von Brentano, P. Nolan, A.J. Kirwan, P.J. Bishop, R. Julin, A. Lampinen, and J. Hattula, Nucl. Phys. **A545**, 822 (1992).
[33] T.K. Alexander and J.S. Forster, Adv. Nucl. Phys. **10**, 197 (1978).
[34] H.P. Hellmeister and L. Lühmann, computer code CRONOS. Göttingen, 1981 (unpublished).
[35] A. Dewald, S. Harissopulos, and P. von Brentano, Z. Phys. A **334**, 163 (1989).
[36] G. Böhm, A. Dewald, P. Petkov, and P. von Brentano, Nucl. Instrum. Methods A **329**, 248 (1993).
[37] P. Möller and J.R. Nix, At. Data Nucl. Data Tables **26**, 165 (1981).
[38] J.A. Becker, S.D. Bloom, and E.K. Warburton, in *Proceedings of the International Symposium On In-Beam Nuclear Spectroscopy,* Debrecen, 1984, edited by Zs. Dombrádi and T. Fényes (Publishing House of the Hungarian Academy of Sciences, Budapest, 1985), p. 737.
[39] E.K. Warburton, J.W. Olness, C.J. Lister, R.W. Zurmühle, and J.A. Becker, Phys. Rev. C **31**, 1184 (1985).
[40] E. Kirchuk, P. Federman, and S. Pittel, Phys. Rev. C **47**, 567 (1993).
[41] E.J. Kaptein, H.P. Blok, L. Hulstman, and J. Blok, Nucl. Phys. **A260**, 141 (1976).
[42] D.H. Gloeckner and F.J.D. Serduke, Nucl. Phys. **A220**, 477 (1974).
[43] F.J.D. Serduke, R.D. Lawson, and D.H. Gloeckner, Nucl. Phys. **A256**, 45 (1976).
[44] K. Oxorn, S.K. Mark, J.E. Kitching, and S.S.M. Wong, Z. Phys. A **321**, 485 (1985).
[45] P.W.M. Glaudemans and P.J. Braussaard, Nucl. Phys. **A102**, 593 (1967).